JOURNAL OF GEOPHYSICAL RESEARCH, VOL. 115, C04020, doi:10.1029/2009JC005524, 2010

High-resolution mapping of Bora winds in the northern Adriatic Sea using synthetic aperture radar

Richard P. Signell,[1,2] Jacopo Chiggiato,[3,4] Jochen Horstmann,[4,5] James D. Doyle,[6] Julie Pullen,[6,7] and Farid Askari[1]

Received 26 May 2009; revised 28 September 2009; accepted 17 November 2009; published 24 April 2010.

[1] The Adriatic Sea is regularly subjected to strong Bora wind events from the northeast during winter. The events have a strong effect on the oceanography in the Adriatic, driving basin-scale gyres that determine the transport of biogeochemical material and extracting large amounts of heat. The Bora is known to have multiple surface wind jets linked to the surrounding orography and have been the focus of many studies, but it has not been possible to describe the detailed spatial structure of these jets by in situ observations. Using high-resolution spaceborne RADARSAT-1 synthetic aperture radar (SAR) images collected during an active Bora period (23 January–16 February 2003), we created a series of high-resolution (300 m) maps of the wind field. The obtained winds show reasonable agreement with several in situ wind observations, with an RMS wind speed error of 3.6 m/s, slightly higher than the 2–3 m/s errors reported in previous studies. These SAR images reveal the spatial structure of the Bora wind in unprecedented detail, showing several new features. In the Senj region of Croatia, several images show rhythmic structure with wavelengths of 2–3 km that may reflect Bora pulsation seen at fixed locations by previous investigators. Along the Italian coast, several images show a wide (20–30 km) band of northwesterly winds that abruptly change to the northeasterly Bora winds further offshore. Meteorological model results suggest that these northwesterly winds are consistent with those of a barrier jet forming along the Italian Apennine mountain chain.

Citation: Signell, R. P., J. Chiggiato, J. Horstmann, J. D. Doyle, J. Pullen, and F. Askari (2010), High-resolution mapping of Bora winds in the northern Adriatic Sea using synthetic aperture radar, *J. Geophys. Res.*, *115*, C04020, doi:10.1029/2009JC005524.

1. Introduction

[2] The Bora is a strong, cold, gusty wind that blows intermittently from the northeast during winter in the Adriatic Sea. It is a downslope wind, occurring when cold, dense air builds up behind the mountains that extend along the northeastern side of the Adriatic. With the formation of either a cyclonic depression over the southern Adriatic or a high-pressure system over central Europe, this dense air is forced through the mountain gaps at the passes, spills rapidly downslope, and forms distinct jets offshore of Trieste, Italy, and Bakar/Senj, Karlobag, and Drage, Croatia (Figure 1). Hourly wind speeds in Senj often exceed 17 m/s, with gusts reaching values of 60 m/s [*Belušić et al.*, 2004]. Gale force (>15 m/s) Bora events occur several times a month during winter (November–March) with a duration of 12 h to several days [*Lazić and Tošić*, 1998]. Depending on the strength and duration of the event (determined mainly by larger-scale weather patterns), the jets can be localized within a few kilometers of the coast or can extend completely across the Adriatic.

[3] The Bora dynamics has been investigated in a number of observational, theoretical, and modeling studies. As a member of the downslope wind family, it can basically be described by hydraulic control theory [*Smith*, 1985], with the strong winds being due to wave breaking, a low-level stable layer, or a combination of both. The northeasterly winds are typically confined to the lower troposphere and reverse at higher levels [*Smith*, 1987; *Grubišić*, 2004]. More discussion of the Bora dynamics is given by *Smith* [1987], *Klemp and Durran* [1987], *Grubišić* [2004], *Belušić et al.* [2004], *Jiang and Doyle* [2005], *Gohm* and *Mayr* [2005], and *Dorman et al.* [2006].

[4] The Bora jets have a strong influence on the oceanography in the northern Adriatic. The intense wind stress and wind stress curl associated with these jets set up complex circulation patterns in the northern Adriatic Sea. These patterns vary significantly from event to event, but they

[1]NATO Undersea Research Centre, La Spezia, Italy.
[2]Now at USGS Woods Hole Coastal and Marine Science Center, Woods Hole, Massachusetts, USA.
[3]Servizio Idrometeorologico, ARPA Emilia Romagna, Bologna, Italy.
[4]Now at NATO Undersea Research Centre, La Spezia, Italy.
[5]GKSS Research Center, Geesthacht, Germany.
[6]Naval Research Laboratory, Monterey, California, USA.
[7]Now at Stevens Institute of Technology, Hoboken, New Jersey, USA.

0148-0227/10/2009JC005524

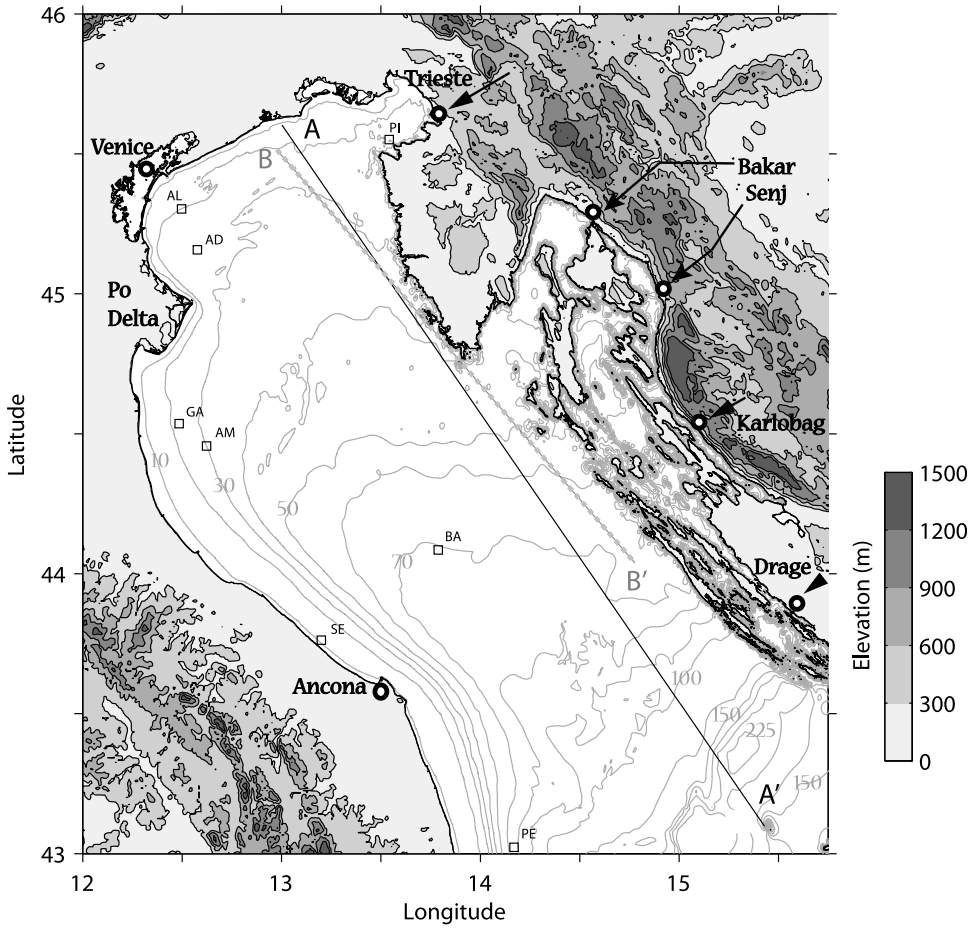

Figure 1. Adriatic Sea regional orography (shading) and bathymetry (contour lines). The thin line A-A′ indicates the transect through the RADARSAT images shown in Figure 7. The dashed line B-B′ indicates the aircraft track flown in the Mesoscale Alpine Programme in 1999 shown in Figure 3.

often have certain repeatable features, confirmed by fixed-moorings drifters, remote sensing, and modeling studies [e.g., *Lee et al.*, 2005; *Kuzmic et al.*, 2007]. Strong southwestward (downwind) flow is generally found under the Bora jets, while northeastward (upwind) flow is found in the weaker wind regions between the jets. In Bora events with well-developed jets at both Trieste and Senj, this results in a counterclockwise gyre to the northernmost Adriatic and a large counterclockwise mid-Adriatic gyre to the south with southeastward flow along the Italian coast (Figure 2). Sometimes a smaller clockwise gyre forms between these two main gyres, trapped against the Istrian peninsula. Beneath the Bora jets, the cold, dry airflow produces severe (>700 W/m^2) heat loss in the water, playing an important role in the production of Northern Adriatic Dense Water, the densest (σ_t > 29.8) water in the Mediterranean Sea [*Malanotte-Rizzoli and Bergamasco*, 1983; *Vilibić and Supić*, 2005].

[5] Oceanographers have long been interested in obtaining a realistic description of the Bora wind fields for the purposes of accurate oceanographic modeling. *Kuzmic and Orlic* [1987] and *Orlić et al.* [1994] were the first to drive a three-dimensional circulation model with a climatological representation of a Bora with a strongly varying lateral wind structure and simulated the multiple-gyre response in the northern Adriatic. *Bergamasco and Gačić* [1996] also demonstrated the importance of Bora structure on circulation by conducting an idealized modeling study, analytically generating a simple banded wind stress field to represent the Bora jets. *Beg Paklar et al.* [2001] showed that with a limited-area meteorological model at 10 km resolution and hydrodynamic model at 2.5 km resolution they were able to reproduce a northern Adriatic counterclockwise gyre (inferred from advanced very high resolution radiometer images) during a specific Bora event. *Pullen et al.* [2003] and *Signell et al.* [2005] showed that limited-area meteorological models (with scales of 4 and 7 km) can represent the distinct jets that characterize the Bora response, while larger-scale models (greater than 20 km resolution) cannot. *Kuzmic et al.* [2007] used a 4 km Coupled Ocean/Atmosphere Mesoscale Prediction System (COAMPS) wind model with a 1 km U.S. Navy Operational Global Ocean Model and a higher-resolution unstructured mesh QUODDY ocean model to show that the double-gyre circulation is sensitive to both atmosphere and ocean model resolution.

[6] Despite the ability of meteorological models to represent the general temporal and spatial characteristics of the Bora jets, there is some evidence of additional features not

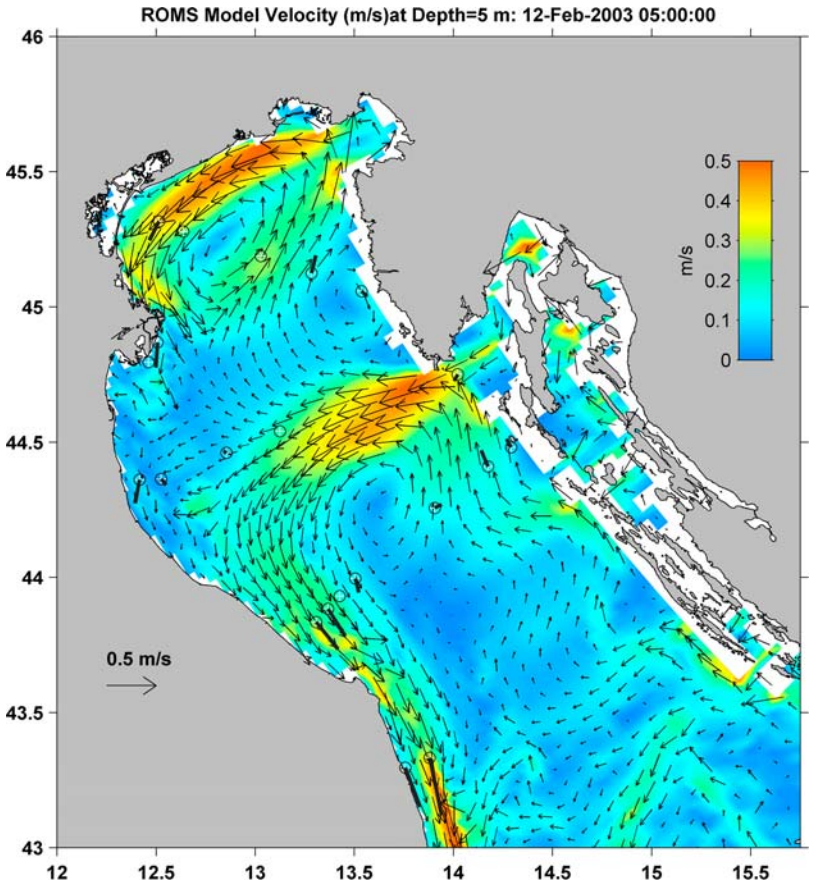

Figure 2. Circulation at 5 m depth from the Ocean Modeling System (ROMS) hydrodynamic and sediment transport model described by *Harris et al.* [2008]. Observations at 5 m depth from acoustic Doppler current profiler moorings described by *Book et al.* [2007] are shown as thick black arrows.

represented by the models. An example of the temporal structure was given by *Belušić et al.* [2004, 2006], who found significant gusts at 1–10 min scales. An example of the more detailed spatial structure was obtained by airborne transect at 200 m altitude during the Mesoscale Alpine Programme in 1999 (Figure 3). Also shown is the wind speed from the 4 km COAMPS model. The transect shows abrupt transitions at the edge of the jets, with changes of 10 m/s over 1 km. Also evident are signs of significant structure within the jets, with variation of several meters per second over scales of several kilometers. It is clear that there is more spatial variability than represented in the model. This transect raises a number of interesting questions: Is similar spatial variability seen on the sea surface? How much variation is there among Bora events? What would the surface wind field look like if it were mapped with a resolution of several hundred meters? These questions can be addressed by using high-resolution satellite-borne synthetic aperture radar (SAR) imagery.

[7] Since the launch of the European remote-sensing satellites ERS-l, ERS-2, and Envisat, as well as the Canadian satellites RADARSAT-1 and more recently RADARSAT-2, SAR images have been acquired over the oceans on a continuous basis over the last 15 years. Their high resolution and large spatial coverage make them a valuable tool for measuring oceanographic parameters such as ocean surface winds, waves, currents, and sea ice. These SAR sensors measure the backscatter primarily caused by ocean roughness at the 5–10 cm scale, roughness that increases with wind speed. Methods developed to invert this relationship have been refined through numerous studies and are now believed to be accurate to 2–3 m/s in the wind speed range 0–20 m/s [*Horstmann et al.*, 2003; *Monaldo et al.*, 2004a, 2004b]. A first look at three SAR images acquired by Envisat during Bora events in the Adriatic Sea revealed a number of interesting structures that could not be obtained by other means: the surface signature of atmospheric gravity waves, strong spatial variations between events, and indications of a possible barrier jet along the Italian coast [*Alpers et al.*, 2009].

[8] As part of a joint research program between NATO and the U.S. Naval Research Laboratory, 10 RADARSAT-1 images were collected over the Adriatic Sea during the 24 day period from 23 January to 16 February 2003. These images spanned the entire northern Adriatic with a pixel resolution of 50 m. RADARSAT-1 acquired imagery on demand and needed to be scheduled well in advance of the range of weather forecasts. This winter period was therefore strategically chosen to maximize the likelihood of capturing Bora winds. We were fortunate in that we obtained Bora wind features on 6 of our 10 images. Preliminary findings from this work were reported by *Askari and Signell* [2004]. We describe here the findings on the structure of the Bora

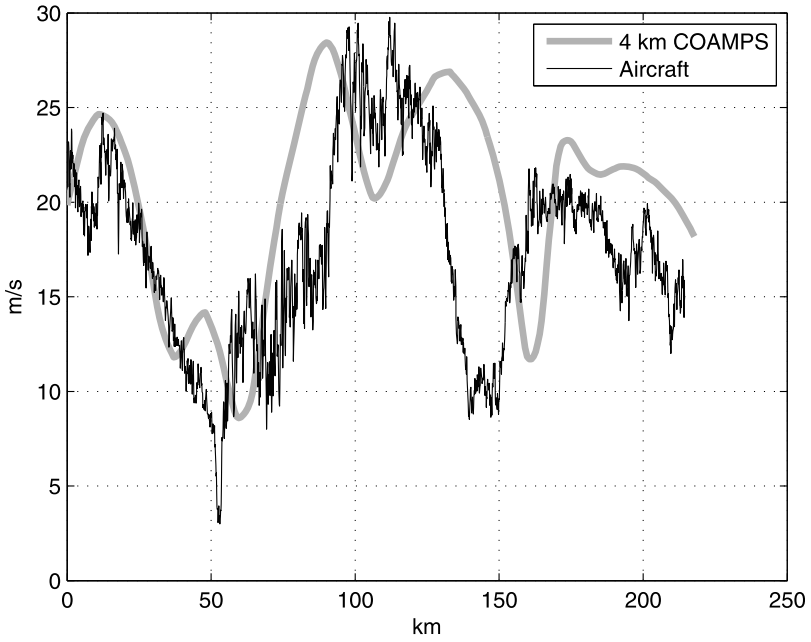

Figure 3. Wind speed measurements at 200 m height acquired during the Mesoscale Alpine Programme along the B-B′ transect depicted in Figure 1. COAMPS, Coupled Ocean/Atmosphere Mesoscale Prediction System.

determined from these images and examine the ability of meteorological models to represent these events.

2. Methods

2.1. Synthetic Aperture Radar (SAR)-Derived Winds

[9] The RADARSAT-1 satellite operates in a near-circular polar and Sun-synchronous orbit at a mean altitude of 790 km. It has an orbital period of 101 min and operates in a 24 day repeat cycle. This SAR system is a right-looking system, which means that the imagery is acquired on the right-hand side with respect to the satellite flight direction (azimuth) perpendicular to the flight direction. RADARSAT-1 acquires images in the C band (5.3 GHz) using horizontal polarization in transmission and reception.

[10] The 10 scenes were acquired in the ScanSAR wide-swath "mode A," which offers the largest coverage in the across-track direction (range). ScanSAR images are generated by scanning over the incidence angles and sequentially synthesizing images for different subswaths. Four beams (W1, W2, W3, and S7) comprise the swath, which cover incidence angles between 20° and 49° in range direction. Each processed image covers an area of approximately 500 km × 500 km, with a pixel size of 50 m. The spatial resolution of the image varies from 86.5 to 146.8 m in range and from 93.1 to 117.5 m in azimuth. All 10 RADARSAT-1 ScanSAR data considered in this study were processed in Gatineau, Canada, at the Canadian Data Processing Facility into ScanSAR images and delivered to us in CEOS format. Each of the CEOS format files contained a single grid of 8-bit integers along with georeferencing, incidence angle, and calibration parameters to allow conversion from raw values into σ_0, the calibrated backscatter intensity. The value σ_0 is also commonly referred to as normalized radar cross section.

[11] For spaceborne microwave radars operating at C band at moderate incidence angles, the backscatter σ_0 is typically largest when the wind blows directly toward the radar and decreases to a minimum when the wind direction is orthogonal to the radar look direction. A smaller maximum in σ_0 occurs when the wind blows directly away from the radar. The relation between the near-surface wind vector and σ_0 can be described by

$$\sigma_0 = a(\theta)u^{\gamma(\theta)}(1 + b(u,\theta)\cos\Phi + c(u,\theta)\cos 2\Phi), \qquad (1)$$

where σ_0 is the normalized radar cross section, u is the wind speed, Φ is the relative angle between the radar look and the wind direction, and θ is the nadir incidence angle. The quantities $a(\theta)$, $\gamma(\theta)$, $b(u,\theta)$, and $c(\theta)$ are empirical parameters that are functions of θ and sometimes u. A number of different functional forms have been proposed, as described below. Equation (1) captures the nature of the relationship of wind vector to backscatter: specifically, that σ_0 is an exponential function of wind speed and a harmonic function of its direction (relative to the radar look direction). Equation (1) specifies σ_0 as a function of wind speed and direction, but we seek wind speed as a function of σ_0. If wind direction can be determined, it is possible to invert equation (1) to obtain wind speed from σ_0. Although one approach is to use predicted wind directions from operational meteorological models [*Monaldo et al.*, 2001], here we prefer to estimate the wind direction directly from linear structures in the SAR image [*Horstmann et al.*, 2002] so that the results depend only on the data, not on the choice of model.

[12] We were fortunate to obtain Bora events in many of our 10 RADARSAT-1 images, the dates of which, as mentioned before, needed to be selected in advance (in the fall of 2002). On the basis of a comparison to the component of northeast wind from the Piran buoy in the Gulf of Trieste,

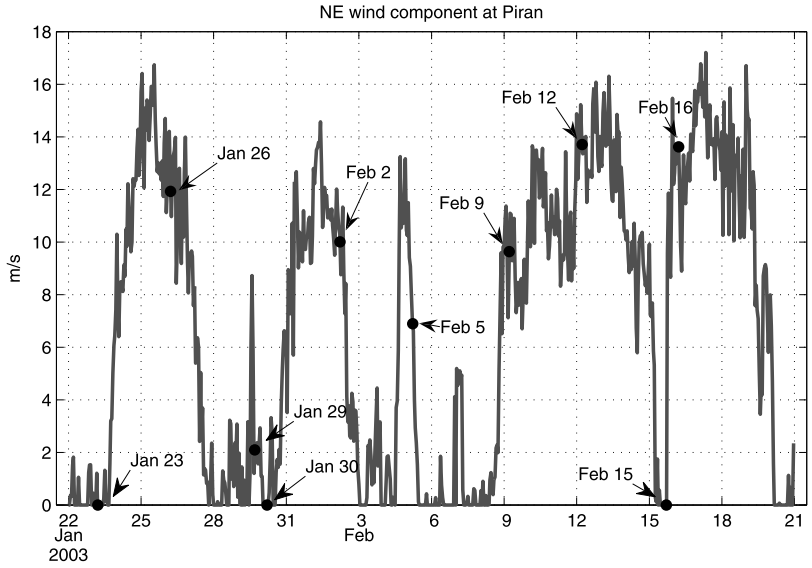

Figure 4. Northeast component of wind observed at the Piran buoy (PI in Figure 1) in the Gulf of Trieste, with the RADARSAT collection times indicated. Values less than 0 (wind from the southwest) are not plotted.

the 26 January and 2, 9, 12, and 16 February images all occurred during typical 2–3 day Bora events (Figure 4). The 5 February image was captured on the tail end of a shorter-duration Bora event, and the 15 February image was captured just at the onset of the 16 February event. With five images we cannot perform meaningful statistics on the patterns of Bora winds, but we have enough to show some range of similarity and differences in the patterns.

2.1.1. Wind Direction Retrieval

[13] The most common methodology for SAR wind direction retrieval is to determine the orientation of linear features at scales above 200 m. Most of these features are associated with wind-induced streaks and marine atmospheric boundary layer rolls. Investigations of tower-based real aperture radar imagery have shown that wind-induced streaks can be seen at various scales between approximately 50 and 500 m [*Dankert et al.*, 2003]. These results suggest focusing on the smallest possible scales that can be utilized from spaceborne SARs, which are ~200 m (limited by the spatial resolution of the SAR system). Results of SAR wind direction retrieval based on larger-scale features (<3 km) often depict boundary layer rolls, which are more likely to differ significantly from the mean surface wind direction [*Etling and Brown*, 1993]. The orientation of the linear features imaged by the SAR can be retrieved by several methods, including the local gradient method [*Horstmann et al.*, 2002; *Koch*, 2004], which is applied in the spatial domain, the fast Fourier transformation method [*Gerling*, 1986; *Fetterer et al.*, 1998; *Lehner et al.*, 1998], which is applied in the spectral domain, and a wavelet technique [*Du et al.*, 2002].

[14] In the Adriatic, we applied the local gradient method with the SAR image smoothed and reduced to resolutions of 100, 200, and 400 m. This results in three SAR images representing spatial scales above 200, 400, and 800 m. From each of these images, local directions (defined by the normal to the local gradient) are computed, leaving a 180° ambiguity. Fortunately, in the Adriatic, we do not encounter this ambiguity issue because Bora winds are always from the northeast quadrant except along the Italian coast, where, as we discuss later, winds sometimes occur from the northwest.

2.1.2. Wind Speed Retrieval

[15] Once the wind direction has been determined, equation (1) can be inverted to determine the wind speed from the backscatter σ_0. For C band σ_0 acquired at vertical polarization in transmit and receive mode, a number of different algorithms have been proposed, each with different functional relationships for the empirical parameters. The most common C band algorithms are the CMOD4 [*Stoffelen and Anderson*, 1997], CMOD_IFR2 [*Quilfen et al.*, 1998], and the recently developed CMOD5 [*Hersbach et al.*, 2007]. Each of these algorithms is directly applicable for wind speed retrieval from C band, vertically polarized SAR images [e.g., *Vachon and Dobson*, 1996; *Lehner et al.*, 1998; *Horstmann et al.*, 2003; *Horstmann and Koch*, 2005].

[16] Although numerous algorithms have been proposed for vertically polarized SAR images, RADARSAT-1 uses horizontal polarization, for which no similar well-developed model exists. To meet this deficiency, a hybrid model function has to be applied that consists of one of the prior mentioned empirical models and a polarization ratio [*Horstmann et al.*, 2000; *Thompson and Beal*, 2000; *Vachon and Dobson*, 2000]. The polarization ratio is defined as the ratio of σ_0 obtained at horizontal to that obtained at vertical polarization. The nature of this polarization ratio is an active area of research, and several different algorithms have been proposed [*Thompson et al.*, 1998; *Mouche et al.*, 2005]. The polarization ratio proposed by *Thompson et al.* [1998] neglects wind speed and wind direction dependence and is given by

$$\mathrm{PR} = \frac{(1 + \alpha \tan^2 \theta)^2}{(1 + 2\tan^2 \theta)^2}, \tag{2}$$

Table 1. In Situ Wind Measurement Information[a]

Site	Abbreviation	Position	Height (m)	DT (min)	Source
Ada	AD	44.18 N 12.59 E	15	30	Agip
Amelia-B	AM	44.42 N 12.66 E	26	30	Agip
Annabella	AN	44.23 N 13.08 E	60	30	Agip
Barbara-C	BA	44.08 N 13.78 E	30	30	Agip
Garibaldi-A	GA	44.52 N 12.51 E	30	30	Agip
Pennina	PE	43.02 N 14.16 E	40	30	Agip
Acqua Alta	AL	45.31 N 12.51 E	20	10	ISMAR-CNR
Piran buoy	PI	45.55 N 13.55 E	5	60	MBS-NIB
Senigallia	SE	43.76 N 13.21 E	3	30	ISMAR-CNR

[a]Height is the anemometer height, and DT is the interval between recorded observations. Abbreviations are as follows: ISMAR-CNR, Istituto di Scienze Marine-Consiglio Nazionale delle Ricerche, Venice, Italy; MBS-NIB, Marine Biology Station, National Institute of Biology, Piran, Slovenia.

where α is an empirical parameter. Several different values for α have been suggested. Although *Unal et al.* [1991] suggested a constant value of 0.6 to yield consistency with their measurements, other researchers have found better fits with values ranging between 0.4 and 1.2 [*Horstmann et al.*, 2000; *Vachon and Dobson*, 2000; *Monaldo et al.*, 2001; *Horstmann and Koch*, 2005]. Comparisons of RADARSAT-1 SAR imagery produced from different SAR processing facilities showed that the different estimates of α might be due to the different radiometric calibrations of RADARSAT-1 SAR data. *Mouche et al.* [2005] proposed that the polarization ratio should be dependent not only on the incidence angle equation (2), but also on wind direction. Their model was constructed using airborne real aperture radar data acquired at C band with both vertical and horizontal polarization for moderate incidence angles and a wide range of wind speeds and wind directions.

[17] The performance of the various algorithms for inverting wind speed based on backscatter varies. Comparisons of C band SAR retrieved wind speeds using the CMOD4 at low to moderate winds (up to ~20 m/s) resulted in errors of ~2 m/s [*Monaldo et al.*, 2001, 2004b; *Horstmann et al.*, 2003; *Horstmann and Koch*, 2005]. Wind speeds obtained using CMOD4 and CMOD_IFR2 models for higher winds (>20 m/s), however, are biased low [*Donnelly et al.*, 1999; *Horstmann et al.*, 2005]. The CMOD5 model was specifically designed to perform better at higher wind speeds. It was constructed primarily using colocations between ERS-2 SCAT backscatter triplets and European Centre for Medium-Range Weather Forecasts (Reading, England) first-guess model winds. For extremely high wind conditions, results from aircraft campaigns were included [*Donnelly et al.*, 1999]. Differences among CMOD4, CMOD5, and CMOD_IFR2 for low to moderate wind speeds are relatively minor. Because of the uncertainty of which algorithm to apply to our Adriatic SAR data, we tested the three different wind speed algorithms (CMOD4, CMOD_IFR2, and CMOD5), each with three different polarization ratio models [*Thompson et al.*, 1998] using $\alpha = 0.6$, $\alpha = 1.0$, and the model suggested by *Mouche et al.* [2005], resulting in a total of nine different algorithms.

[18] It is worth pointing out that all these methods assume neutral stability to obtain a relationship between wind speed at 10 m height and wind stress at the sea surface. The backscatter σ_0 is actually caused by the wind stress at the sea surface, but the algorithms for σ_0 have been developed using the wind speed. Compared to stable and neutral conditions, the same wind in unstable conditions will generate a higher wind stress at the sea surface and therefore a higher σ_0, resulting in a higher SAR retrieved wind speed [e.g., *Zecchetto et al.*, 1998]. In unstable conditions, such as those that occurred during the strong winter cooling conditions found here, the SAR algorithms may derive wind speeds that are slightly too high. Investigations of *Dankert and Horstmann* [2007] using a real aperture radar showed that the stability of the marine boundary layer can lead to significant biases in radar wind speed retrieval. Tests with the Coupled Ocean-Atmosphere Response Experiment 3.0 [*Fairall et al.*, 2003] momentum flux routines using observations (air temperature, sea temperature, atmospheric pressure, relative humidity, and wind speed) from the Acqua Alta platform, however, suggest that this bias for these images is less than 5%.

2.2. Observed Winds

[19] Direct wind measurements were obtained from a variety of sources. Since our primary interest was in assessing wind over the ocean, for quantitative comparison with the SAR data we used data from all the offshore sources we could find: six Agip offshore gas platforms, the Istituto di Scienze Marine-Consiglio Nazionale delle Ricerche (CNR-ISMAR) oceanographic platform Acqua Alta, the Piran oceanographic buoy, and the CNR-ISMAR oceanographic buoy at Senigallia (Figure 1 and Table 1). Because the data was collected at various heights, we first converted the data to equivalent wind at 10 m assuming a log layer and neutral stability. The averaging interval was also variable: 10 min for Acqua Alta and Senigallia (stations AL and SE in Figure 1), 30 min for the Agip platforms, and 60 min for Piran (station PI in Figure 1).

2.3. Comparing SAR-Derived and Observed Winds

[20] Comparing SAR-derived winds to observed winds requires special consideration. The observed wind is a point measurement in space but was averaged over varying lengths of time (from 10 to 60 min). The SAR-derived wind is averaged over 300 m in space but is essentially a point measurement in time (each 300 m cell is imaged for about 1 s). In addition, SAR returns very high backscatter off the platforms, which yields very high wind values at the exact location of the wind measurements on the platforms. It is therefore necessary to perform spatial averaging of the SAR data. The simplest method was to take the median value of the SAR wind in a box of a certain size centered on the observed wind locations. Taking the median allowed the high returns from the cells with platforms to be eliminated. We tried box sizes from 900 m (9 cells) to 3300 m (111 cells). We also tried an approach in which we used the frozen turbulence hypothesis, averaging the SAR winds over a swath length that would pass by in 10 min if the wind moved with the constant speed and direction observed at the sensor. For example, if the observed wind was 10 m/s from the northeast, we compared this wind to SAR-derived wind averaged over a 6 km long, 300 m wide swath (10 m/s × 10 min × 60 s/min = 6000 m) oriented in the NE/SW direction and centered on the sensor location. The correlation between SAR-derived and observed winds increased with box from

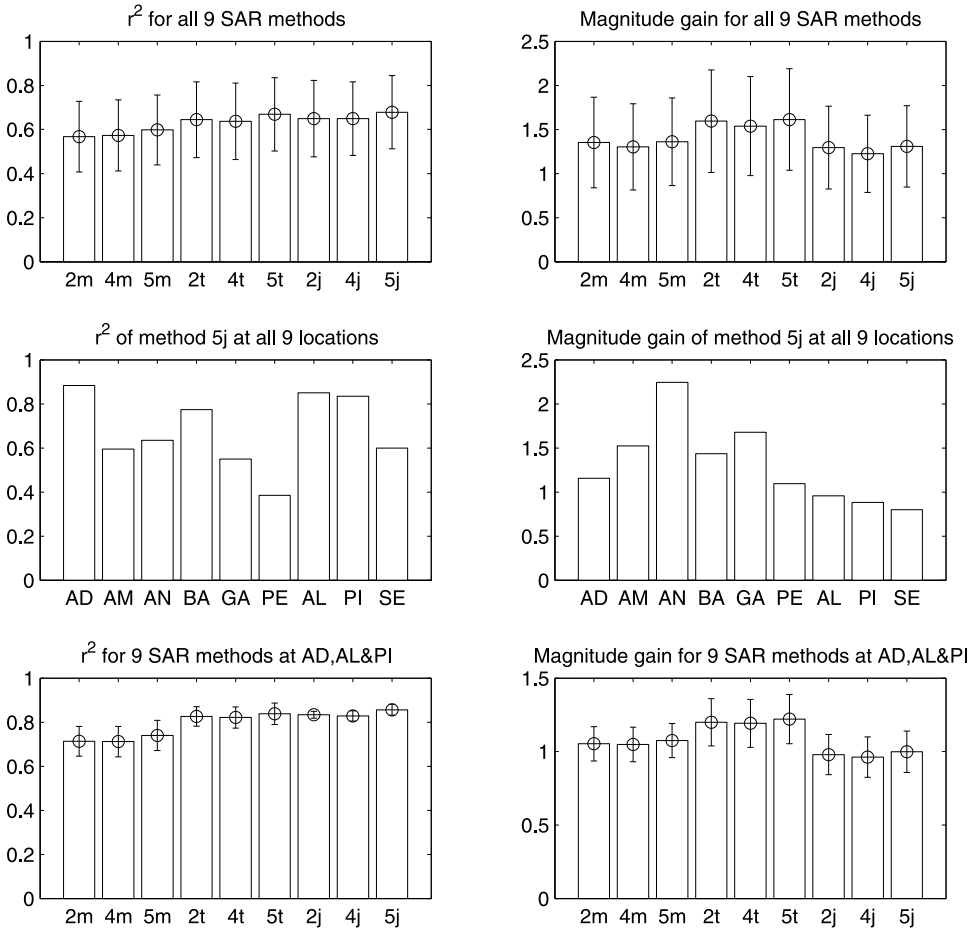

Figure 5. Correlation and magnitude gain for the different synthetic aperture radar (SAR) algorithms. The two-character code indicates the basic algorithm and the type of polarization ratio scheme used: 2, 4, and 5 indicate CMOD_IFR2, CMOD4, and CMOD5 respectively, and m, t, and j indicate the polarization ratio scheme of *Mouche et al.* [2005], α = 0.6, and α = 1.0, respectively. For example, 2m indicates CMOD_IFR2 with the Mouche polarization ratio method. See Table 1 for site abbreviations.

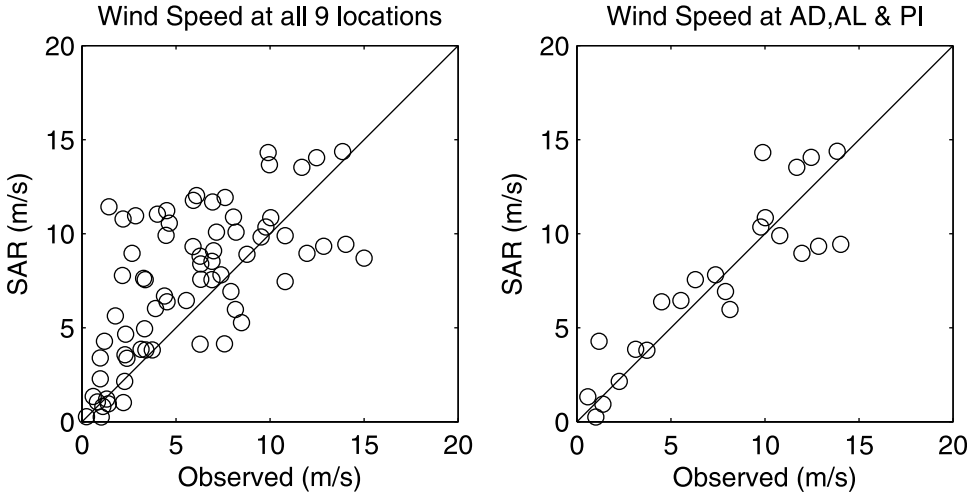

Figure 6. Scatterplot of SAR-derived wind speeds versus observations for (a) all stations and (b) the stations Ada (AD), Acqua Alta (AL), and Piran (PI).

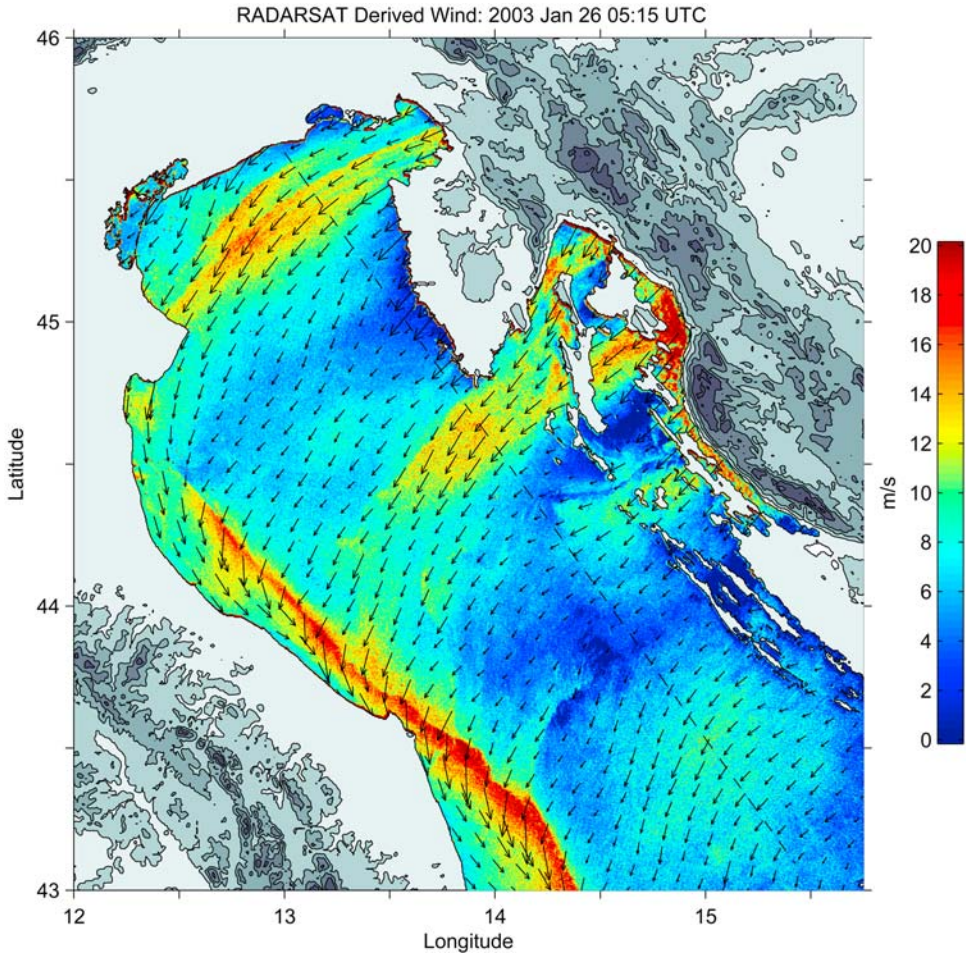

Figure 7. (a) SAR-derived wind field at 0515 UTC on 26 January 2003, along with the orography surrounding the Adriatic Sea. The dashed line indicates the location of the section shown in Figures 8 and 9. The typical alternating jet-and-wake structure due to interaction of the Bora with the eastern complex topography is clearly seen, along with the dual-jet nature of the Trieste jet. A coastal band of strong northwest wind is seen running along the western Adriatic coastline. (b) SAR-derived wind field at 0511 UTC on 2 February 2003. The Trieste jet is oriented more easterly as compared to 26 January and has a broader maximum. A northwest wind structure is again found along the western coastline but is much smaller extent than in the 26 January image. (c) SAR-derived wind field at 0507 UTC on 9 February 2003. (d) SAR-derived wind field at 0521 UTC on 12 February 2003. The dual-jet nature of the Trieste Jet is again evident, and northeasterly winds are present over the entire northern Adriatic. (e) SAR-derived wind field at 0505 UTC on 16 February 2003. This is the strongest Bora event recorded by our 10 SAR images, with winds reaching 20 m/s in the Gulf of Trieste. The Trieste jet again has a dual-jet nature.

900 to 2100 m, then remained constant to 3300 m. The more sophisticated frozen-turbulence swath method did not give significantly improvement over the 2100 m result. Thus we opted for the simple 2100 m box median results for assessing the performance of the nine different SAR algorithms.

2.4. Numerical Atmospheric Models

2.4.1. Limited Area Model Italy

[21] The Limited Area Model Italy (LAMI) is the Italian operational implementation of the Lokal Model (LM) [*Steppeler et al.* [2003], a limited-area model originally developed by the German Weather Service (DWD) for mesoscale and microscale weather prediction and simulation. LM has continued to be developed by several European meteorological services belonging to the Consortium for Small Scale Modeling. LAMI is managed by the Hydrometeorological Service of the Emilia-Romagna Regional Agency for Environmental Protection (ARPA), the Ufficio Generale per la Meteorologia, Italian Airforce, and ARPA Piemonte. It has been operational since the beginning of 2001 at the CINECA Supercomputing Centre in Bologna, Italy. LAMI is a fully compressible, nonhydrostatic 3-D model with 7 km grid spacing and 35 vertical terrain-following levels in which initial and boundary conditions are obtained from the DWD global circulation model GME [*Majewsky et al.*, 2002]. At the time of this research, LAMI

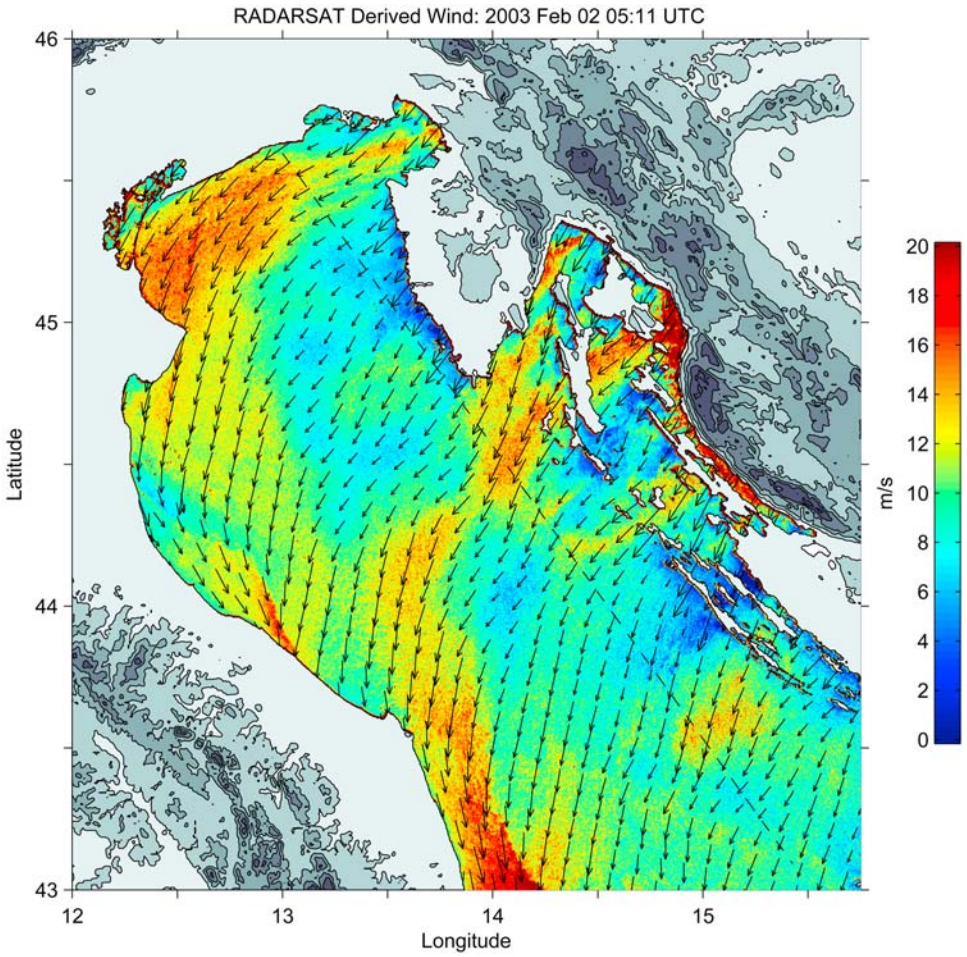

Figure 7. (continued)

gave output every 3 h with 48 h forecast length once a day. Forecast winds from hours 3–24 were used to construct a continuous 3-hourly wind time series.

2.4.2. Coupled Ocean/Atmosphere Mesoscale Prediction System Model

[22] COAMPS is a 3-D, finite-difference, nonhydrostatic, sigma-coordinate model developed by the Naval Research Laboratory [*Hodur*, 1997]. The version adopted was run in a reanalysis mode using three nested grids with the finest 4 km grid mesh centered over the Adriatic Sea. The two outer meshes are a 12 km grid covering the majority of the Mediterranean and a 36 km resolution European grid. The global Navy Operational Global Atmospheric Prediction System provides lateral boundary conditions for the 36 km grid at 6 h intervals. In the reanalysis configuration, analyses are performed twice daily with forecasts for the following 15 h. Forecast winds from hours 3–14 were used to construct a continuous hourly wind time series. Further details of the COAMPS Adriatic reanalysis are documented by *Pullen et al.* [2003, 2007].

2.5. Selecting a SAR Algorithm

[23] We attempted to determine the best SAR algorithm by comparing the correlation and magnitude gain among the nine different SAR algorithms considered and the observed wind at the platform and buoys. Using the SAR winds computed from the 2.1 km box median and observed wind converted to 10 m height, we calculated the regression coefficient and slope between these two variables using the nine different locations and 10 different SAR images. We forced the fit through zero so that the slope of the line indicates the magnitude gain: the degree to which the wind speeds are overpredicted or underpredicted by the SAR algorithm (e.g., a slope of 1.1 means that SAR-derived winds are 10% too high). We also computed standard regression that was not forced through zero and confirmed that it did not change the nature of the findings.

[24] With the overall data set, we are not able to statistically distinguish the best method based on correlation or magnitude gain, as the error bars all overlap. The r^2 value range is 0.57–0.68, and the magnitude gain range is 1.22–1.61 (Figures 5a and 5b). At some stations, however, the correlation is much better than at others. Looking at the nine stations individually for the 5j algorithm (CMOD5 with α = 1.0), we find that stations AD (Ada platform), AL (Acqua Alta platform), and PI (Piran buoy) have correlations above 0.8 and amplitude gains in the range 0.88–1.15 (Figures 5c and 5d). Two of these locations (Acqua Alta and Piran) are

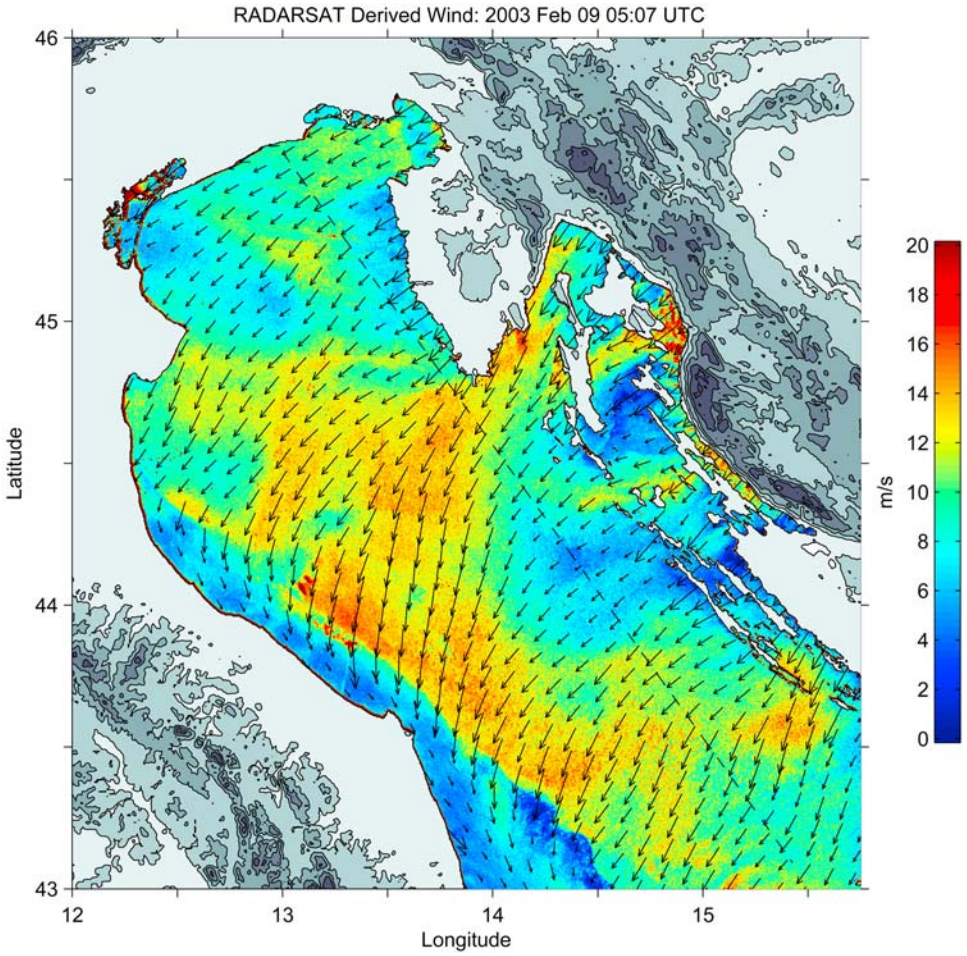

Figure 7. (continued)

stations carefully maintained by oceanographic institutions, which might account for the better performance. In addition, some of the poorer-performing stations are in regions where the Bora is more variable, where larger errors in wind speed could be due to larger errors in the SAR estimation of wind direction. If we use only these three best stations for the purpose of determining the best SAR algorithm (Figures 5e and 5f), we find that the 5j algorithm has the highest correlation, $r^2 = 0.85$, and the magnitude gain closest to 1 (0.99). We therefore selected the CMOD5 algorithm with $\alpha = 1.0$ as the "best" scheme for our purposes and used it for the rest of the analysis and figures in this paper. The degree of scatter obtained with this algorithm (and all the other algorithms) is relatively large for the data set as a whole (Figure 6a), with an RMS error of 3.6 m/s. Much of the SAR error is in the lower observed wind speeds, where there are many anomalously high SAR winds indicated. The scatter is considerably less at the best-fitting stations such as Piran, Acqua Alta, and Ada (Figure 6b). The RMS error for these three stations is 2.0 m/s, nearly twice as small as for the overall group and agrees with typical findings of other researchers.

3. Results

[25] The SAR wind fields obtained during the five Bora events on 26 January and 2, 9, 12, and 16 February 2003 are fascinating in the detailed features they describe and in both their similarities and differences (Figure 7). On all images, several strong jets of northeast winds can be seen extending downstream of the Dinaric Alps, but the number and intensity of the jets vary markedly with each image. There are basically four main jet regions, associated with gaps in the mountains to the northeast of Trieste, Bakar/Senj, Karlobag, and Drage.

[26] The intensity and lateral structure of these jets can be quantified by taking a slice of wind speed (Figure 8) along the track A-A′ shown in Figure 1. For the 16 February event we can see that all four jets are strong (wind speeds greater than 14 m/s) and well defined. Considerable variation can be seen within the jets as well. In particular, the Trieste jet has two distinct maxima of 18 and 20 m/s separated by a distance of about 20 km. The boundaries of the jets can be quite sharp. On the north side of the Bakar/Senj jet, the wind changes by 8 m/s in 10 km. The relative vorticity banner associated with this jet would therefore have a magnitude of at least 8×10^{-4} s^{-1}. The structure of the wind speed along this section is strikingly similar to that obtained by aircraft measurements shown in Figure 3, including the two distinct maxima of the Trieste jet.

[27] From the 10 km smoothed transects from all five Bora events (Figure 9), the Trieste and Bakar/Senj jets are

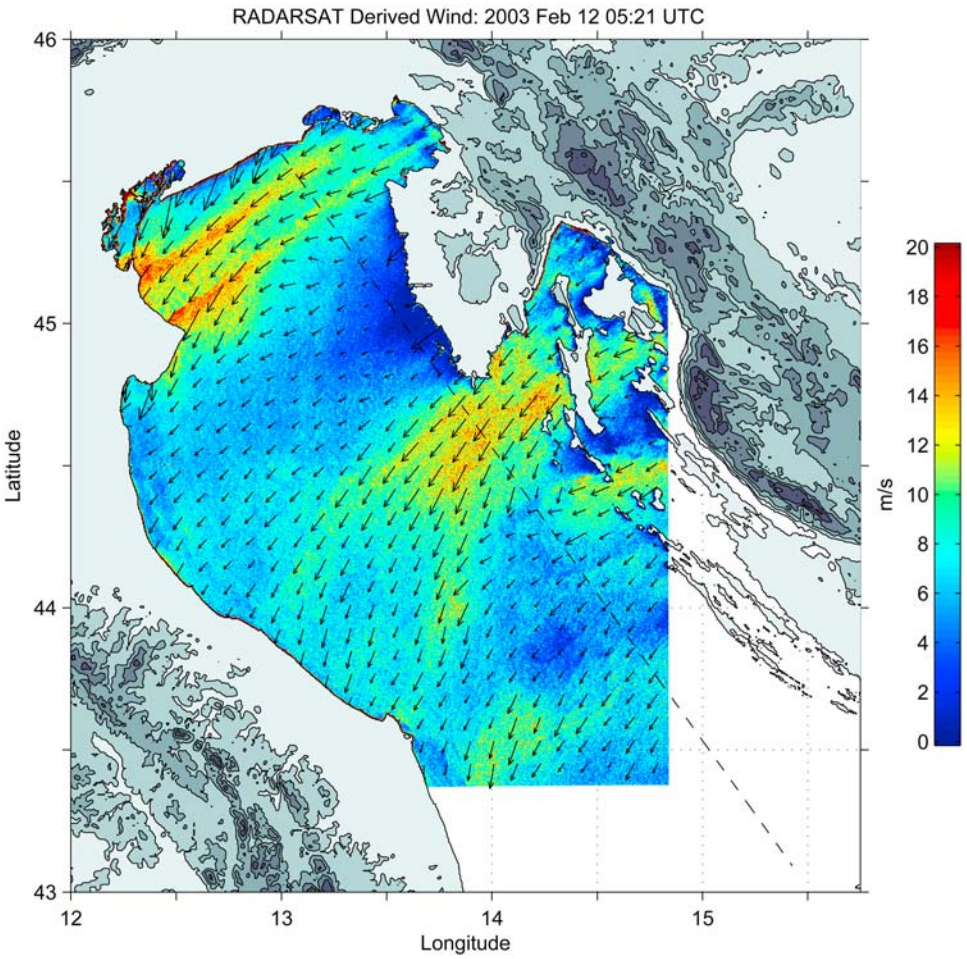

Figure 7. (continued)

the most dominant and show up clearly in the five-event mean. The Drage jet is weaker but also shows up clearly in the five-event mean. The Karlobag jet, in contrast, is sometimes very strong, as in the 16 February image, but it is sometimes nonexistent, as in the 9 February image. As a result, it does not appear in the five-event mean.

[28] In addition to the northeast Bora wind jets, several images (26 January and 2 and 9 February) reveal bands of northwest wind along the Italian coast. In the following sections we describe the wind structure in each region and the bands of wind along the Italian coast.

3.1. The Trieste Jet

[29] The northeast wind jet originating in the Gulf of Trieste is found in all five of the Bora events. This jet extends across the entire northern Adriatic to the Po Delta, with peak speeds exceeding 12 m/s; it reaches 20 m/s in the 16 February event. There are some significant differences in the Trieste jet structure, however. In the 2 and 9 February images, the jet is rather broad and diffuse, and the maximum winds extend to the northern coast of the Adriatic. In the 26 January and 12 and 16 February 16 images, however, the Trieste jet is very distinct and is composed of two bands of wind with distinct offshore maxima.

[30] A closer look at the Gulf of Trieste region shows weaker winds in the northern part of the gulf and stronger winds in the southern part (Figure 10). The banding appears in every image except 9 February, and the variations in speed are substantial. In the 2, 9, and 12 February images there is also a region of reduced wind about 10 km offshore, possibly reflecting a jump of the type reported by *Gohm and Mayr* [2005] and *Gohm et al.* [2008]. The image on 15 February is remarkable, as it captures the leading edge of the Bora jet as it moves across the Gulf of Trieste just after onset in Trieste. The image was taken at 1652 UTC. At 1700 UTC the Piran buoy was recording calm winds below 0.4 m/s (see Figure 4), consistent with the SAR image. One hour after the image was obtained, however, at 1800 UTC, the wind speed at Piran increased to 9.6 m/s. Further to the west, the Aqua Alta anemometer showed the Bora arrived at 2150 UTC, and by 0505 UTC on 16 February (the time of our last SAR image), the Bora was fully developed, 10 h after onset.

3.2 The Bakar and Senj Jets

[31] The Bakar and Senj jet region also shows many similarities and differences between images (Figure 11). In the north, off Bakar, there are strong winds in all but the 12 February image. In the images on 26 January and 2 and

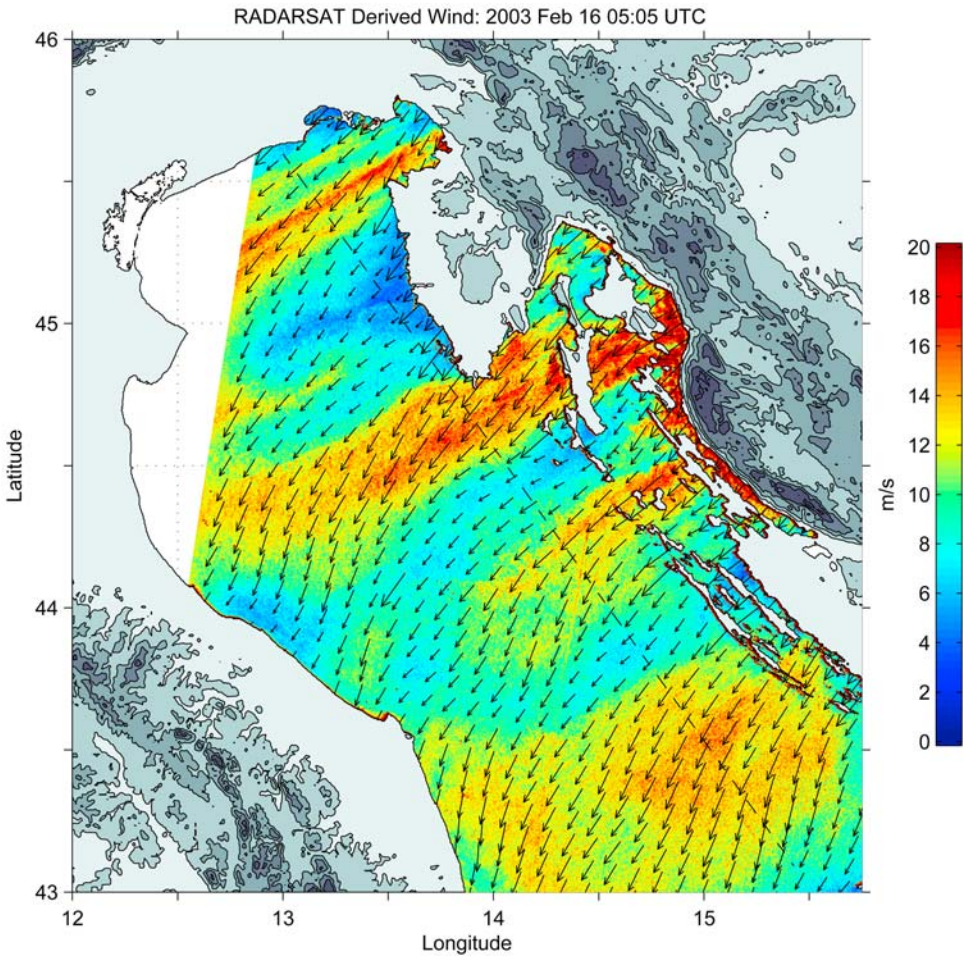

Figure 7. (continued)

15 February, a narrow band of very strong wind (20 m/s) extends westward across the bay (near to Bakar) and shows distinct rhythmic variations in the speed in the along wind direction. With a single snapshot, we cannot distinguish between standing lee waves and propagating waves. If they were waves propagating with the mean wind speed of 15 m/s, the wavelength of 2 km would correspond to about 2 min pulsation in time measured at a fixed location. These features may reflect the same phenomena reported by *Belušić et al.* [2006], who saw distinct pulsation in the 1–10 min band from high-frequency wind measurements at Senj. In the 12 February image, which displayed no such periodic features, there is a low-wind region between Senj and Krk. *Belušić et al.* [2007] found that in a high-resolution simulation of this region, in the case with no wind pulsations, they observed weak surface winds with reversed direction between Senj and Krk. Although we cannot distinguish between downwind and upwind winds when the wind speed is low, this low-wind region could be consistent with the model findings.

[32] In all six images the strongest winds occur along the coast near Senj, and the jet emanating from this region flows southwestward in a 10–15 km wide band over the islands. Immediately to the northwest there is a low-wind-speed region, which results from sheltering effects of the high mountains upwind. The Bakar and Senj jets appear to coalesce downstream of Cres Island, forming the broad, strong jet that reaches out into the Adriatic. The occurrence of distinct jets in the island region is also a feature of the subkilometer-resolution model simulations of *Gohm and Mayr* [2005] and *Gohm et al.* [2008].

3.3. The Apennines Barrier Jet

[33] While two of the Bora images show northeast winds across the entire northern Adriatic (12 and 16 February), the other three images (26 January and 2 and 9 February) reveal a dramatic change in the wind direction in a band along the Italian coast. The size and the strength of the wind in this band vary, but the wind is northwesterly in all three images and has a strong front at the offshore boundary. We suspect that these patterns are caused by a barrier jet that forms on the windward side of mountain chains, in this case the Apennine mountain chain that runs along the western Adriatic coast.

[34] The 26 January image reveals perhaps the most dramatic Italian coastal feature. In this image a northwesterly wind band extends 10–20 km off along the Italian coast south of the Po Delta. The winds in this wide band are approximately normal to the northeasterly Bora winds offshore, representing an abrupt 90° change in wind direction. The abrupt change in wind direction determined by the

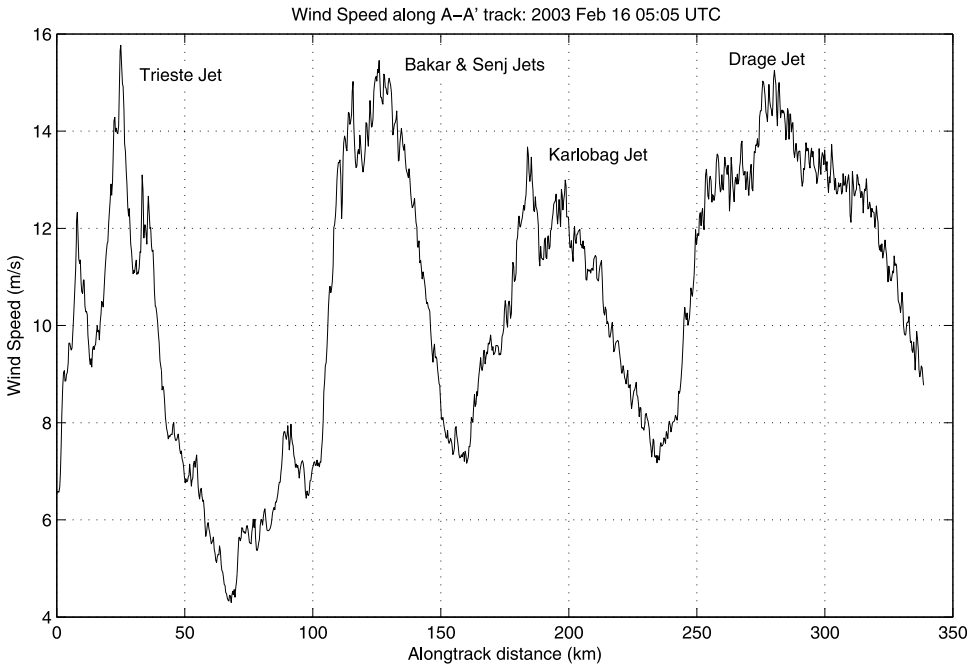

Figure 8. SAR-derived wind speed for 16 February 2003 along section A-A′ shown in Figure 1 and indicated by a dashed line in Figure 7.

WISAR algorithm is verified by the wind direction recorded at nearby stations (Figure 12).

[35] The offshore boundary of this band would seem to show a 1–2 km band of very strong winds, approaching 20 m/s. Closer analysis of this image, however, revealed that this strong wind at the frontal boundary is an artifact of the automatic wind direction algorithm. Because this algorithm must analyze streaks over a sizable region (5 km), the wind direction field is significantly smoother than the backscatter field at the front. Because the backscatter depends strongly

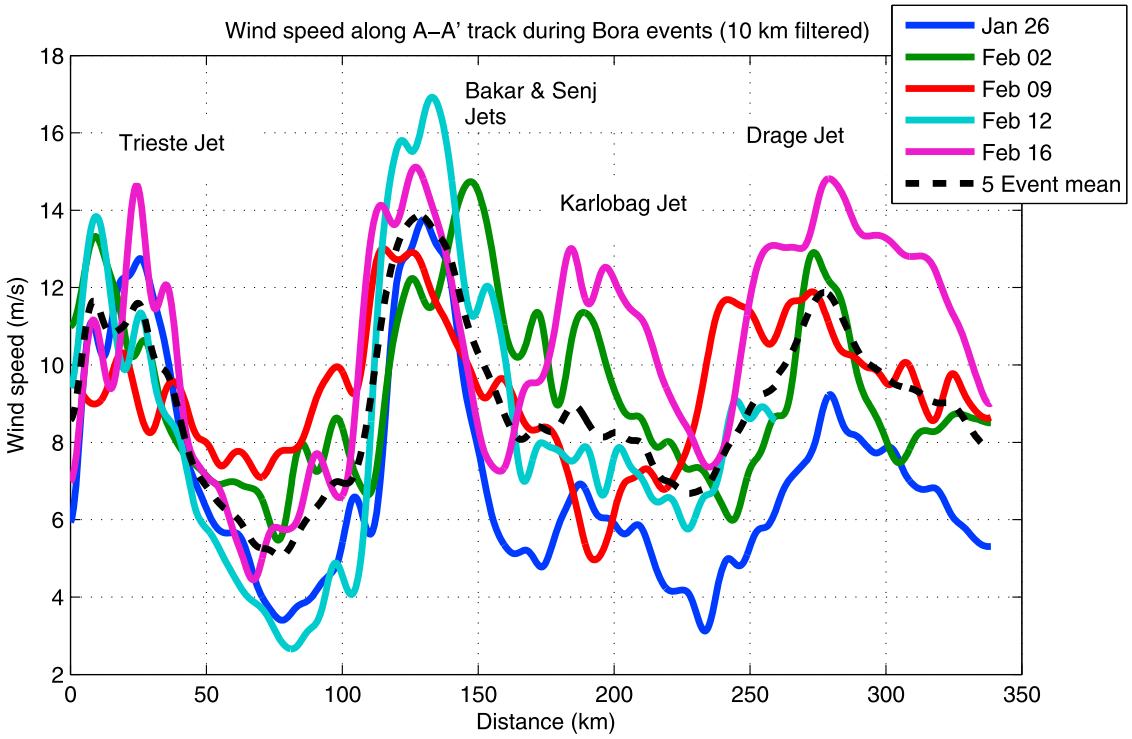

Figure 9. Smoothed (10 km) SAR-derived wind speed for all five Bora events along section A-A′ shown in Figure 1 and indicated by a dashed line in Figure 7.

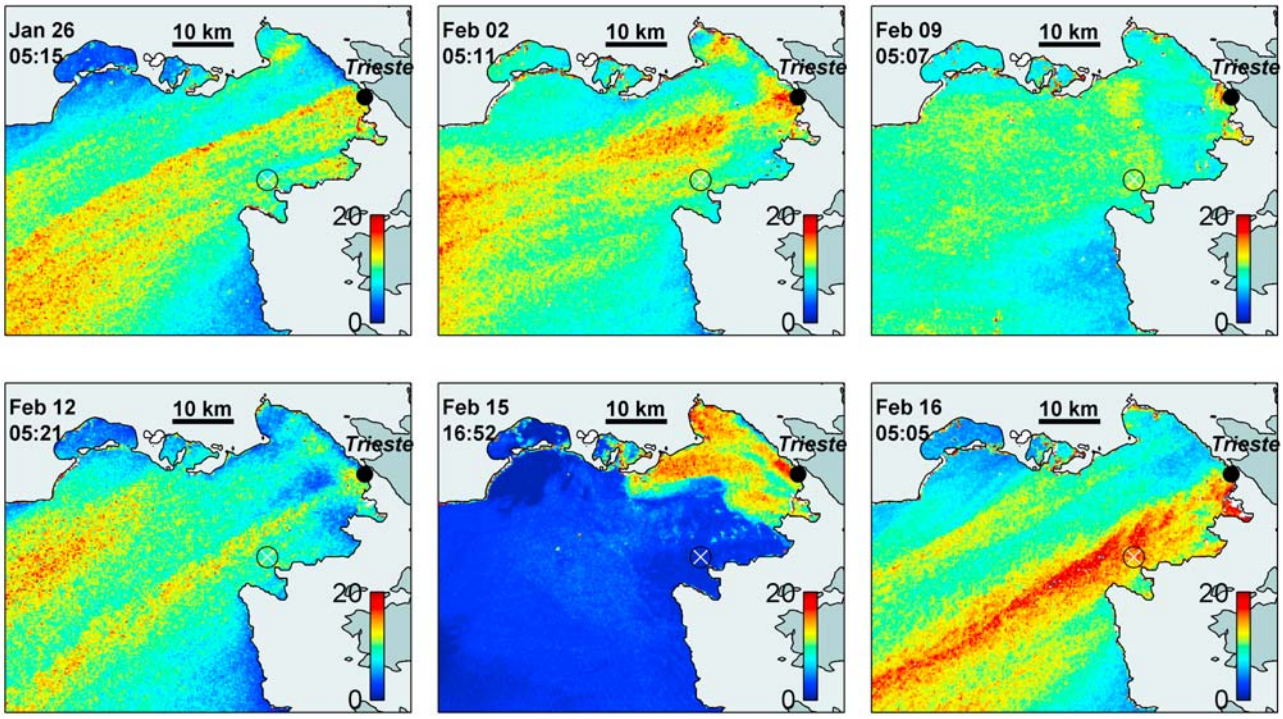

Figure 10. Comparison of SAR-derived wind speeds for six Bora events in the Gulf of Trieste region. The location of the Piran oceanographic buoy is indicated.

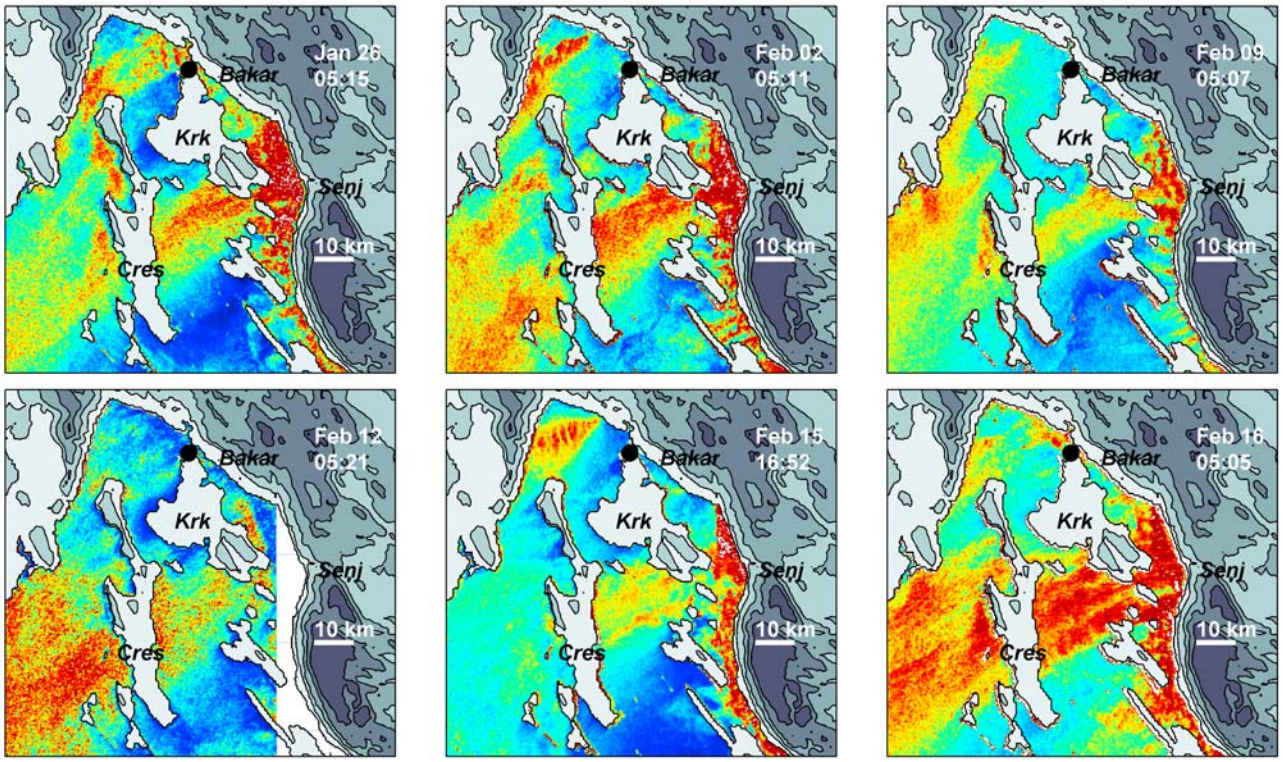

Figure 11. SAR-derived wind speed during six Bora events in the Bakar/Senj region. While features such as the strong band of winds from the gap at Senj across the middle of Cres Island are found in all images, other features, such as the rhythmic pattern northwest of Bakar, are more sporadic.

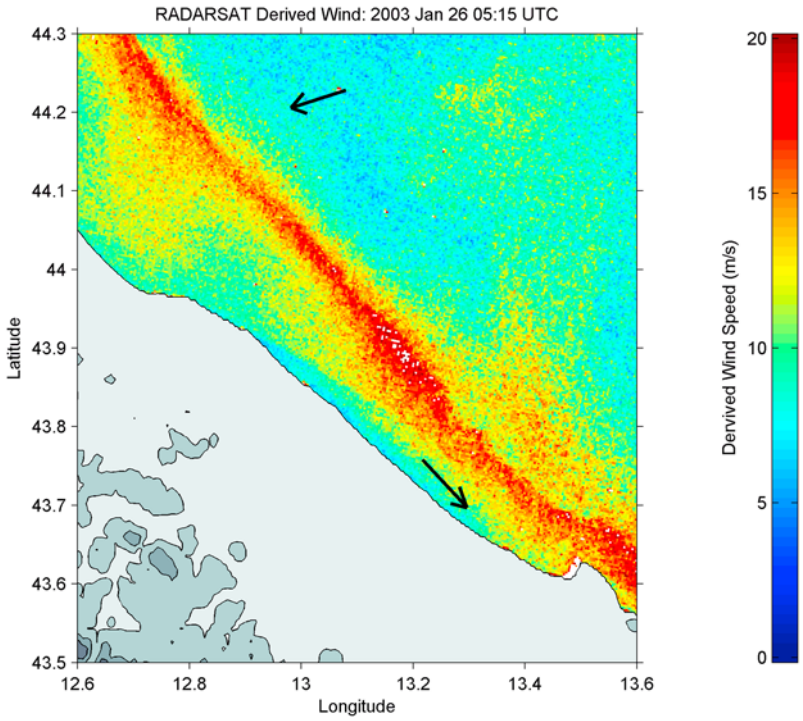

Figure 12. Detail of a region near the Italian coast at 0515 UTC on 26 January 2003. Observations of local wind direction are shown by the arrows, consistent with the theory that the front seen in the SAR image represents an abrupt change in the wind direction. Because of the smoothing used by the WISAR algorithm to determine wind direction, the wind speed along the frontal boundary is overestimated in this case, as described more fully in the text.

on the wind direction, errors in direction caused by the smoothing result in errors in the wind speed, in this case artificially increasing the wind speeds at the front. We were able to demonstrate that when we manually selected the region shoreward of the front and assigned it a northwest wind direction, no such elevated wind speeds were seen along the front. Special front detection and one-sided wind direction methods would have to be employed in the automatic wind direction scheme to avoid such small-scale artifacts at the frontal boundary. We emphasize that it is only the 1–2 km band of strong wind that is the artifact, not the broad northwesterly wind band itself. We will discuss this feature more in the next section.

[36] The 2 February image also shows bands where the wind suddenly changes from northeast to northwest, although their extent is more limited. The 9 February image shows a wide region where the wind is from the northwest, as on 26 January, but here the wind speed is dramatically reduced.

3.4. Comparison With Wind Fields From Limited-Area Numerical Models

[37] The availability of high-resolution (<10 km) wind fields from numerical models gives us the opportunity to explore the dynamics of the observed patterns when they agree with modeled patterns. At the same time, the very high resolution of the SAR wind fields (300 m) gives us a unique opportunity to assess the numerical models. Typically the modeled wind fields are assessed by comparing them to widely spaced buoy and platform observations, but the SAR winds allow us to assess how well the models can represent the detailed spatial structure of the Bora wind field. *Signell et al.* [2005] showed that high-resolution 4 km COAMPS and 7 km LAMI models could represent and distinguish among the main Bora jets, while lower-resolution models (20 and 45 km) could not. Other authors have also shown that the structure of the alternating jets and wakes is sensitive to model resolution [*Grubišić*, 2004; *Jiang and Doyle*, 2005; *Beg Paklar et al.*, 2001; *Pullen et al.*, 2003]. While increasing model resolution should lead to more accurate representation of the wind field, it is possible that some aspects of the patterns seen in SAR images would require improved physics of boundary layer processes as well.

[38] Comparing the SAR-retrieved wind fields with outputs from the 4 km COAMPS and 7 km LAMI described in section 2.4, we found that the models captured with reasonable accuracy the jet morphology, although there are some noticeable differences. For the 2 February Bora, the two models capture the main structure of the Bora jets, although the Trieste Jet is weaker and further to the south (Figure 13). The COAMPS wind indicates a thin band of northwest wind along the Italian coast as in the SAR image, although the location and shape are somewhat different. The LAMI wind shows no such indication of northwest wind, with northeast wind found across the entire northern Adriatic.

[39] For the 12 February Bora, LAMI has a broader jet shifted to the south relative to the SAR image, and neither model captures the dual-jet structure of the Trieste jet. It

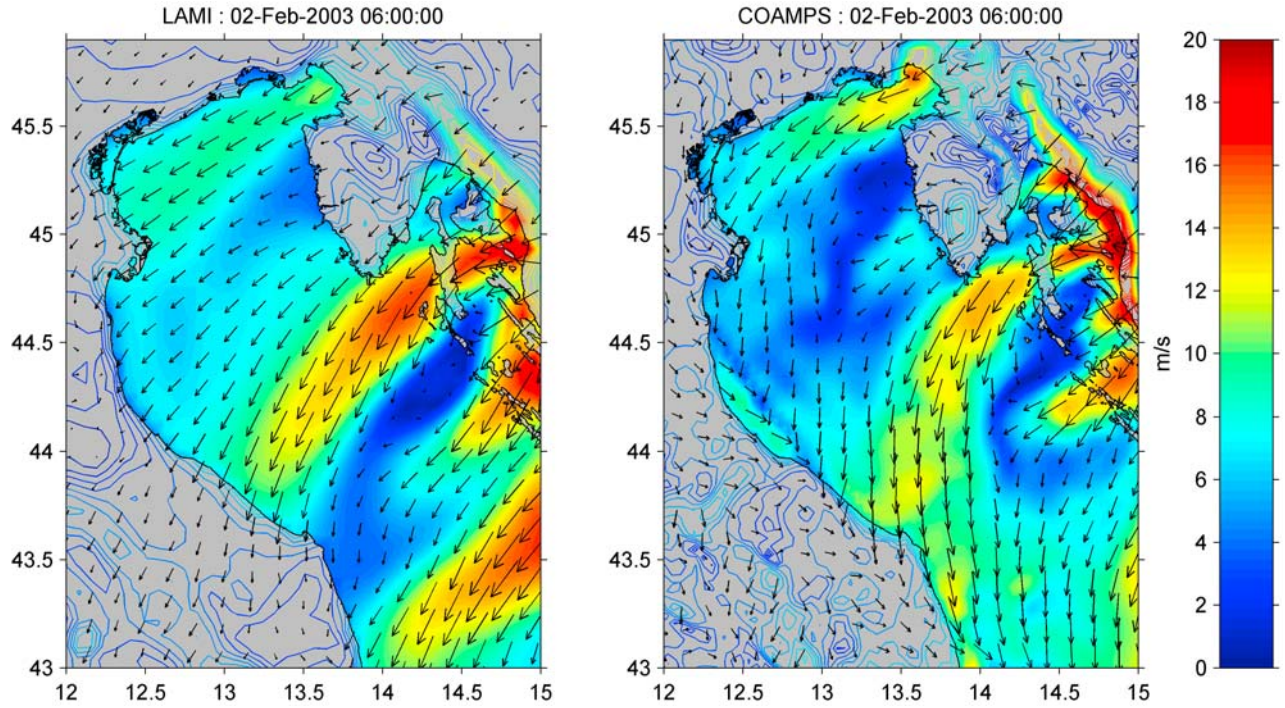

Figure 13. Modeled 10 m wind from (left) Limited Area Model Italy (LAMI) and (right) COAMPS at 0600 UTC on 2 February. Compare with the SAR-derived wind in Figure 7b. The two models capture the main structure of the Bora jets, although the Trieste jet is weaker and further to the south. The COAMPS wind shows a thin band of northwesterly wind along the Italian coast as in the SAR image, although the location and shape are not exactly correct. The LAMI wind shows no such indication of northwesterly winds: northeasterly winds are found across the entire northern Adriatic.

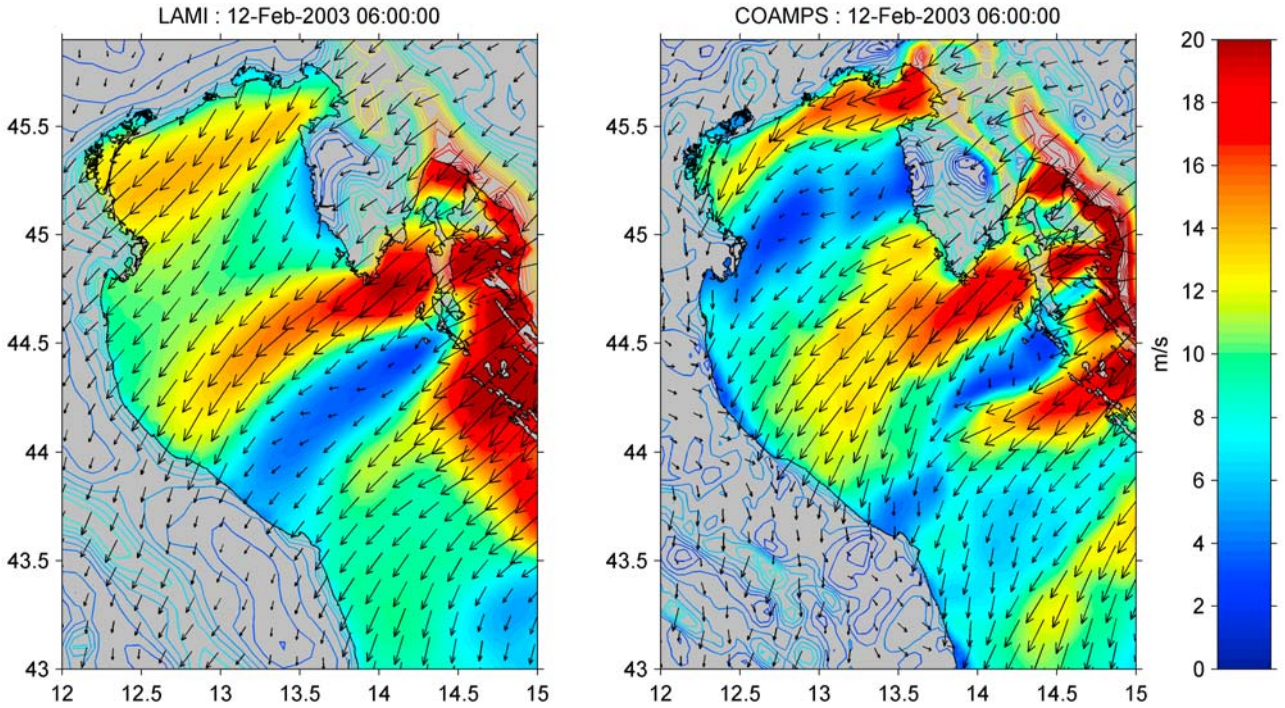

Figure 14. Modeled 10 m wind from (left) LAMI and (right) and COAMPS at 0600 UTC on 12 February 12. Compare with the SAR-derived wind in Figure 7d. The southernmost jet in LAMI is clearly broader. Neither of the models shows a dual-jet nature in the Trieste jet.

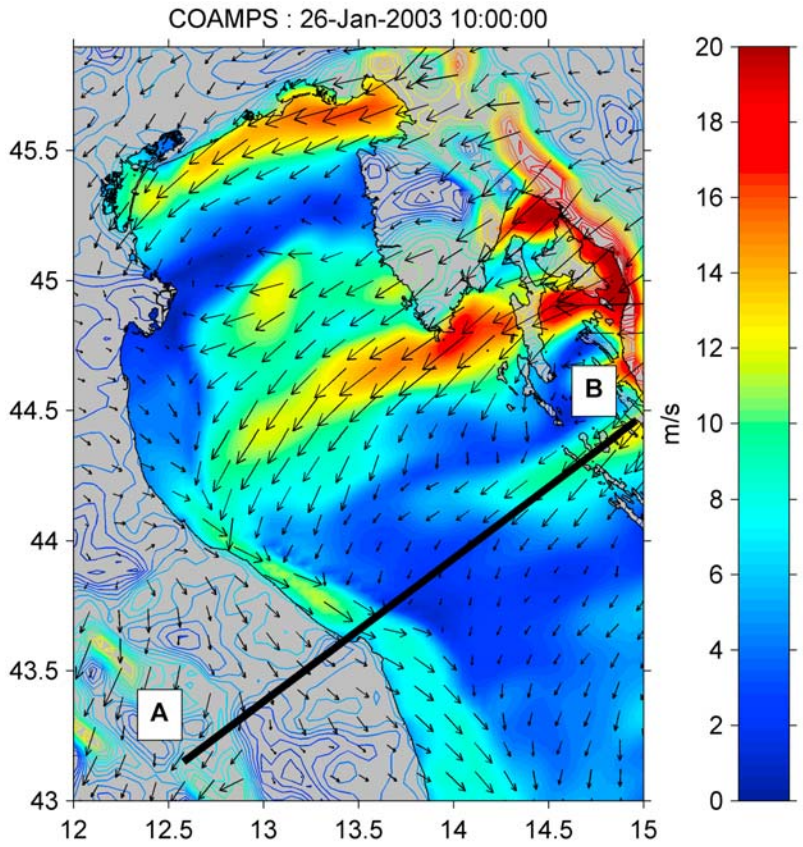

Figure 15. Modeled 10 m wind from COAMPS at 1000 UTC on 26 January. Compare with the SAR-derived wind field in Figure 7a. Although occurring 5 h later, the model clearly shows the band of northwesterly wind along the western Adriatic coastline. The line shows the location of the vertical transect plotted in Figure 16.

may be that this dual-jet structure is due to a very small ridge to the northeast of Trieste that induces a wake region in between the stronger jets. Subkilometer resolution may be necessary to resolve this topography and the resulting dual jet in the Trieste region. This behavior was not seen in the 0.8 km simulations by *Gohm and Mayr* [2005], however. It may be that this behavior was not present during the weak Bora of March 2002 they simulated, or it could be that even more resolution or improved parameterization of boundary layer physics is required.

[40] We can also use the models to explore the nature of the coastal band that appears along the Italian coast. Taking the 26 January event as a representative example, we explore whether the abrupt change in wind direction could be explained by an atmospheric barrier jet, a feature that can form under certain conditions on the windward side of the mountain chain. As discussed by *Parish* [1982], *Doyle* [1997], and *Loescher et al.* [2006], there is a blockage of wind when the oncoming flow perpendicular to a ridge cannot cross over the topographic barrier. In classical barrier jet theory, the normal flow is blocked when the Froude number is less than 1.0, the onshore flow being too stable to ascend the barrier. This creates a damming of cold air toward the barrier, creating an across-barrier pressure gradient and forcing the flow to rotate to the left (Northern Hemisphere) in along the barrier. The maximum distance upstream where the flow begins to feel the topography is the topographic Rossby deformation radius.

[41] The numerical models can be used to explore the barrier jet hypothesis. While at 0600 UTC (the time closest to the SAR image) neither model shows any sign of a coastal jet (Figure 14), by 1000 UTC a remarkably similar structure emerges in the COAMPS model (Figure 15). Such a field is fully consistent with coastal blockage; the calculated average Froude number in the region is 0.8 (less than 1), and a vertical slice through the COAMPS model reveals that there is a dome-shaped mass of cold air pushed toward the coast along with a clear jet (Figure 16). Analysis of other Bora events in the COAMPS simulation show that this barrier jet appears quite frequently. It is worth pointing out that this version of COAMPS (and LAMI) use highly smoothed analysis fields of sea surface temperature, so the models are unable to represent the cold marine coastal current underneath the jet, which enhances even more the stability of the air column above [*Pullen et al.*, 2006]. In the fully coupled air-sea simulation, *Pullen et al.* [2007] showed that the barrier jets in this region tend to form in the early morning hours, reflecting differential cooling over land relative to the ocean. Errors such as the 4–5 h lag in the development of the barrier jet in our noncoupled COAMPS

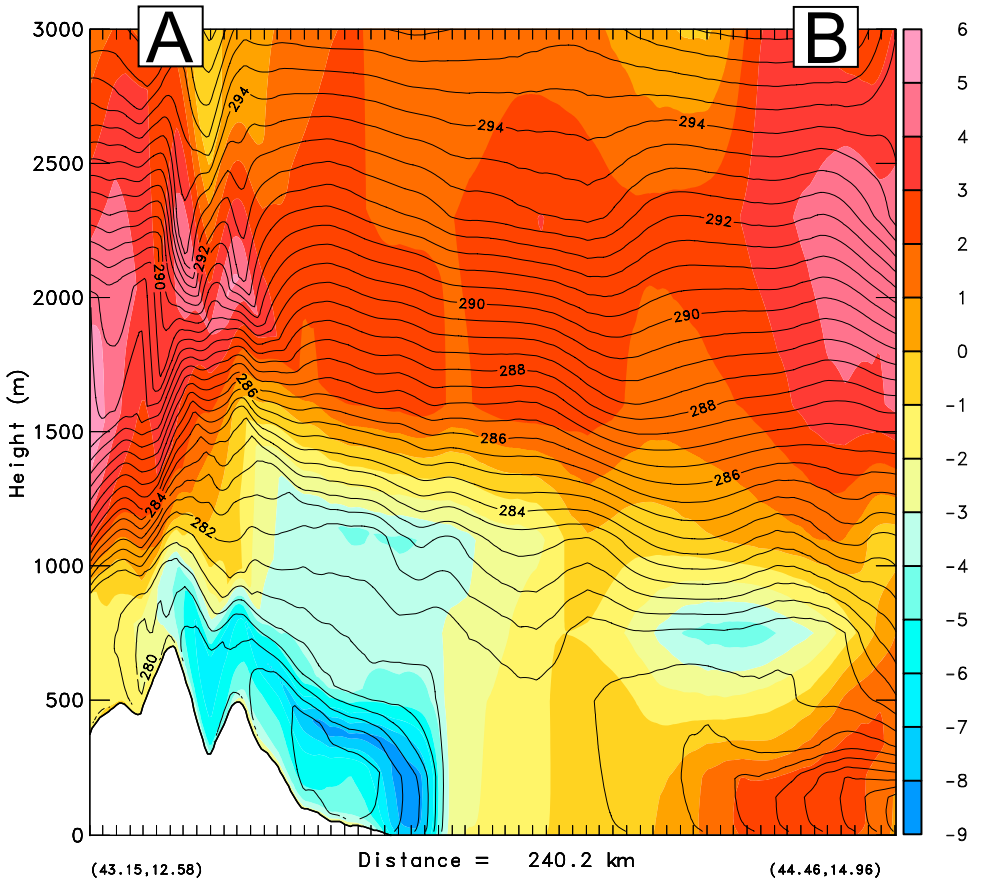

Figure 16. Modeled cross-coast vertical transect from COAMPS at 1000 UTC on 26 January 2003 along the line shown in Figure 15, showing wind speed (meters per second, color scale) normal to the section and potential temperature (contours, interval every 0.5 K). The cross section shows a sloping inversion, cold-air pooled against the mountains, and an along-coast northerly wind, all consistent with barrier jet theory.

model could therefore likely be improved with two-way air-sea coupling.

4. Conclusions

[42] These RADARSAT-1 ScanSAR images have provided fascinating glimpses into the detailed (300 m) spatial structure of Bora winds over the entire northern Adriatic. They have both refined our existing knowledge of the alternating jet and wake pattern and have revealed structures not seen before, such as the dual-jet nature of the Trieste jet, possible pulsations in the Bakar and Senj jet region, and the formation of the barrier jet on the western Adriatic coast. As the wind field maps (Figure 6) and the cross-sectional comparison of wind (Figure 8) make clear, the five Bora events captured here show many differences in addition to similarities. All events have distinct jets, for example, but sometimes one jet distinctly dominates over another or can be missing completely. Attempting to define a mean Bora pattern might therefore have limited merit, as it will be important for the models to capture the appropriate wind pattern for individual events to force realistic circulation patterns.

[43] On the basis of our rather limited data set, the wind speed inversion algorithms developed for the open sea (the CMOD algorithms) appear to work moderately well in the Adriatic. We used median wind from a 2 km footprint in the SAR images to compare with observations, to avoid the high SAR backscatter values from the gas platforms on which many of the wind measurements were collected. Considering three different algorithms, CMOD4, CMOD5, and CMOD_IFR2, we chose the CMOD5 algorithm because it had the best correlation with the observations, although was not statistically different than the other schemes. The root mean square error of the best algorithm (CMOD5) was 3.6 m/s for all wind data but was about 2.0 m/s for the three best-maintained wind stations. Using an a of 1.0 in the polarization ratio suggested by *Thompson et al.* [1998] worked better than the 0.6 used by many investigators, reducing the SAR winds to values much closer to observations. This could also be working as a proxy for Bora winds gustier than the typical conditions that the CMOD algorithms were developed for. If gusty winds produce a rougher surface for a given mean wind speed, the CMOD algorithms based on inversion of this roughness would then overpredict the mean wind speed. More work should be done to explore

this hypothesis. We emphasize that we are not claiming that the CMOD5 algorithm with a polarization of 1.0 is the best algorithm in general for the Adriatic Sea: more data and analysis would be required to make such a claim.

[44] The automatic wind direction method employed by our automatic SAR processing program needs to be refined to handle fronts, to avoid artifacts in the wind speed along frontal boundaries. These artifacts are caused when abrupt changes in wind direction occur over scales that are comparable to the footprint of the streak detection scheme. In these cases, special front detection and one-sided techniques would need to be employed to prevent averaging the wind directions on either side of the front.

[45] Meteorological models at several kilometers resolution can represent the large-scale structures seen in the SAR images rather well, although naturally with some variation in phase (e.g., the barrier jet on 26 January appeared in the model for the first time approximately 4–5 h after the actual jet visible in the SAR-retrieved wind field). These models do not represent the detailed dual-jet nature of the Trieste jet or the several-kilometer-wavelength structures in the Bakar and Senj jet region. To resolve this detail, it is likely that subkilometer models will be necessary and possibly will require improved physics. If these detailed wind fields are resolved, it is not clear what the impact will be on the ocean circulation. *Kuzmic et al.* [2007] showed that the multiple-gyre response to the Bora is very sensitive to meteorological forcing and oceanographic resolution, however, so additional studies along these lines would be warranted. Perhaps the wind structure depicted in the SAR-derived winds could be used for forcing in an idealized fashion (e.g., to examine the response to a steady wind with this spatial structure).

[46] The images collected in this work were exciting in the range of Bora variability they exhibited. It would be highly desirable to obtain a much larger set so that climatology and statistics of these Bora events could be determined. This should now be possible with access to a much larger and growing database and with reduced costs of acquiring SAR data.

[47] **Acknowledgments.** We thank those who provided the meteorological data: Sandro Carniel and Luigi Cavaleri at ISMAR-CNR for the Acqua Alta platform, Vlado Malacic at the National Institute of Biology, Slovenia, for the Piran oceanographic station, Micaela Puletti at Agip for the Agip platforms, and Aniello Russo for the Senigallia buoy. We also thank Danijel Belušić for stimulating discussions concerning this work.

References

Alpers, W., A. Ivanov, and J. Horstmann (2009), Observations of Bora events over the Adriatic Sea and Black Sea by spaceborne synthetic aperture radar, *Mon. Weather Rev.*, *137*, 1150–1161, doi:10.1175/2008MWR2563.1.

Askari, F., and R. P. Signell (2004), RADARSAT mapping of Bora winds in the Adriatic Sea, *Tech. Rep. SR-111*, NATO Undersea Res. Cent., La Spezia, Italy.

Beg Paklar, G., V. Isakov, D. Koraćin, V. Kourafalou, and M. Orlić (2001), A case study of a Bora-driven flow and density changes on the Adriatic Shelf (January 1987), *Cont. Shelf Res.*, *21*, 1751–1783, doi:10.1016/S0278-4343(01)00029-2.

Belušić, D., M. Pasarić, and M. Orlić (2004), Quasi-periodic Bora gusts related to the structure of the troposphere, *Q. J. R. Meteorol. Soc.*, *130*, 1103–1121, doi:10.1256/qj.03.53.

Belušić, D., M. Pasarić, Z. Pasarić, M. Orlić, and B. Grisogono (2006), A note on local and non-local properties of turbulence in the Bora flow, *Meteorol. Z.*, *15*, 301–306, doi:10.1127/0941-2948/2006/0127.

Belušić, D., M. Žagar, and B. Grisogono (2007), Numerical simulation of pulsations in the Bora wind, *Q. J. R. Meteorol. Soc.*, *133*, 1371–1388, doi:10.1002/qj.129.

Bergamasco, A., and M. Gačić (1996), Baroclinic response of the Adriatic Sea to an episode of Bora wind, *J. Phys. Oceanogr.*, *26*, 1354–1369, doi:10.1175/1520-0485(1996)026<1354:BROTAS>2.0.CO;2.

Book, J. W., R. P. Signell, and H. Perkins (2007), Measurements of storm and nonstorm circulation in the northern Adriatic: October 2002 through April 2003, *J. Geophys. Res.*, *112*, C11S92, doi:10.1029/2006JC003556.

Dankert, H., and J. Horstmann (2007), A marine-radar wind sensor, *J. Atmos. Oceanic Technol.*, *24*(9), 1629–1642, doi:10.1175/JTECH2083.1.

Dankert, H., J. Horstmann, and W. Rosenthal (2003), Ocean wind fields retrieved from radar-image sequences, *J. Geophys. Res.*, *108*(C11), 3352, doi:10.1029/2003JC002056.

Donnelly, W. J., J. R. Carswell, R. E. McIntosh, P. S. Chang, and J. Wilkerson (1999), Revised ocean backscatter models at C and Ku band under high wind conditions, *J. Geophys. Res.*, *104*, 11485–11498, doi:10.1029/1998JC900030.

Dorman, C. E., et al. (2006), February 2003 marine atmospheric conditions and the Bora over the northern Adriatic, *J. Geophys. Res.*, *111*, C03S03, doi:10.1029/2005JC003134.

Doyle, J. D. (1997), The influence of mesoscale orography on a coastal jet and rainband, *Mon. Weather Rev.*, *125*, 1465–1488, doi:10.1175/1520-0493(1997)125<1465:TIOMOO>2.0.CO;2.

Du, Y., P. W. Vachon, and J. Wolfe (2002), Wind direction estimation from SAR images of the ocean using wavelet analysis, *Can. J. Remote Sens.*, *28*, 498–509.

Etling, D., and R. Brown (1993), Roll vortices in the planetary boundary layer: A review, *Boundary Layer Meteorol.*, *18*(3), 215–248, doi:10.1007/BF00705527.

Fairall, C. W., E. F. Bradley, J. E. Hare, A. A. Grachev, and J. B. Edson (2003), Bulk parameterization of air-sea fluxes: Updates and verification for the COARE algorithm, *J. Clim.*, *16*, 571–591, doi:10.1175/1520-0442(2003)016<0571:BPOASF>2.0.CO;2.

Fetterer, F., D. Gineris, and C. Wackerman (1998), Validating a scatterometer wind algorithm for ERS-1 SAR, *IEEE Trans. Geosci. Remote Sens.*, *36*(2), 476–492, doi:10.1109/36.662731.

Gerling, T. (1986), Structure of the surface wind field from Seasat SAR, *J. Geophys. Res.*, *91*(C2), 2308–2320, doi:10.1029/JC091iC02p02308.

Gohm, A., and G. J. Mayr (2005), Numerical and observational case-study of a deep Adriatic Bora, *Q. J. R. Meteorol. Soc.*, *131*, 1363–1392, doi:10.1256/qj.04.82.

Gohm, A., G. J. Mayr, A. Fix, and A. Giez (2008), On the onset of Bora and the formation of rotors and jumps near a mountain gap, *Q. J. R. Meteorol. Soc.*, *134*, 21–46, doi:10.1002/qj.206.

Grubišić, V. (2004), Bora-driven potential vorticity banners over the Adriatic, *Q. J. R. Meteorol. Soc.*, *130*, 2571–2603, doi:10.1256/qj.03.71.

Harris, C. K., C. R. Sherwood, R. P. Signell, A. J. Bever, and J. C. Warner (2008), Sediment dispersal in the northwestern Adriatic Sea, *J. Geophys. Res.*, *113*, C11S03, doi:10.1029/2006JC003868.

Hersbach, H., A. Stoffelen, and S. de Haan (2007), An improved C-band scatterometer ocean geophysical model function: CMOD5, *J. Geophys. Res.*, *112*, C03006, doi:10.1029/2006JC003743.

Hodur, R. (1997), The Naval Research Laboratory's coupled ocean/atmosphere mesoscale prediction system, *Mon. Weather Rev.*, *125*, 1414–1430, doi:10.1175/1520-0493(1997)125<1414:TNRLSC>2.0.CO;2.

Horstmann, J., and W. Koch (2005), Measurement of ocean surface winds using synthetic aperture radars, *J. Oceanic Eng.*, *30*(3), 506–515.

Horstmann, J., W. Koch, S. Lehner, and R. Tonboe (2000), Wind retrieval over the ocean using synthetic aperture radar with C-band HH polarization, *IEEE Trans. Geosci. Remote Sens.*, *38*(5), 2122–2131, doi:10.1109/36.868871.

Horstmann, J., W. Koch, S. Lehner, and R. Tonboe (2002), Ocean winds from RADARSAT-1 ScanSAR, *Can. J. Remote Sens.*, *28*, 524–533.

Horstmann, J., H. Schiller, J. Schulz-Stellenfleth, and S. Lehner (2003), Global wind speed retrieval from SAR, *IEEE Trans. Geosci. Remote Sens.*, *41*(10), 2277–2286, doi:10.1109/TGRS.2003.814658.

Horstmann, J., D. R. Thompson, F. Monaldo, S. Iris, and H. C. Graber (2005), Can synthetic aperture radars be used to estimate hurricane force winds? *Geophys. Res. Lett.*, *32*, L22801, doi:10.1029/2005GL023992.

Jiang, Q., and J. D. Doyle (2005), Wave breaking induced surface wakes and jets observed during a Bora event, *Geophys. Res. Lett.*, *32*, L17807, doi:10.1029/2005GL022398.

Klemp, J. B., and D. R. Durran (1987), Numerical modeling of Bora winds, *Meteorol. Atmos. Phys.*, *36*, 215–227, doi:10.1007/BF01045150.

Koch, W. (2004), Directional analysis of SAR images aiming at wind direction, *IEEE Trans. Geosci. Remote Sens.*, *42*(4), 702–710, doi:10.1109/TGRS.2003.818811.

Kuzmic, M., and M. Orlic (1987), Wind induced vertical shearing: ALPEX/MEDALPEX data and modeling exercise, *Ann. Geophys.*, *5B*, 103–112.

Kuzmic, M., I. Janekovic, J. W. Book, P. J. Martin, and J. D. Doyle (2007), Modeling the northern Adriatic double-gyre response to intense Bora wind: A revisit, *J. Geophys. Res.*, *111*, C03S13, doi:10.1029/2005JC003377.

Lazić, L., and I. Tošić (1998), A real data simulation of the Adriatic Bora and the impact of mountain height on Bora trajectories, *Meteorol. Atmos. Phys.*, *66*, 143–155, doi:10.1007/BF01026630.

Lee, C., et al. (2005), Northern Adriatic response to a wintertime Bora wind event, *Eos Trans. AGU*, *86*(16), 157, 163, 165, doi:10.1029/2005EO160001.

Lehner, S., J. Horstmann, W. Koch, and W. Rosenthal (1998), Mesoscale wind measurements using recalibrated ERS SAR images, *J. Geophys. Res.*, *103*(C4), 7847–7856, doi:10.1029/97JC02726.

Loescher, K. A., G. S. Young, B. C. Colle, and N. S. Winstead (2006), Climatology of barrier jets along the Alaskan coast: Part I. Spatial and temporal distributions, Mon. *Weather Rev.*, *134*, 437–453, doi:10.1175/MWR3037.1.

Majewsky, D., D. Liermann, P. Prohl, B. Ritter, M. Buchhold, T. Hanisch, G. Paul, W. Wergen, and J. Baumgardner (2002), The operational global icosahedral-hexagonal gridpoint model GME: Description and high resolution tests, *Mon. Weather Rev.*, *130*, 319–338, doi:10.1175/1520-0493(2002)130<0319:TOGIHG>2.0.CO;2.

Malanotte-Rizzoli, P., and A. Bergamasco (1983), The dynamics of the coastal region of the northern Adriatic sea, *J. Phys. Oceanogr.*, *13*, 1105–1130, doi:10.1175/1520-0485(1983)013<1105:TDOTCR>2.0.CO;2.

Monaldo, F. M., D. R. Thompson, R. C. Beal, W. G. Pichel, and P. Clemente-Colòn (2001), Comparison of SAR-derived wind speed with model predictions and ocean buoy measurements, *IEEE Trans. Geosci. Remote Sens.*, *39*, 2587–2600, doi:10.1109/36.974994.

Monaldo, F., D. Thompson, W. Pichel, and P. Clemente-Colon (2004a), A systematic comparison of QuikScat and SAR ocean surface wind speeds, *IEEE Trans. Geosci. Remote Sens.*, *42*(2), 283–291, doi:10.1109/TGRS.2003.817213.

Monaldo, F., et al. (2004b), The SAR measurement of ocean surface winds: An overview, in *Proceedings of the Second Workshop on Coastal and Marine Applications of SAR*, edited by H. Lacoste, pp. 15–32, Eur. Space Agency, Noordwijk, Netherlands.

Mouche, A., D. Hauser, J.-F. Daloze, and C. Guerin (2005), Dual polarization measurements at C-band over the ocean: Results from airborne radar observations and comparison with ENVISAT ASAR data, *IEEE Trans. Geosci. Remote Sens.*, *43*(4), 753–769, doi:10.1109/TGRS.2005.843951.

Orlić, M., M. Kuzmić, and Z. Pasarić (1994), Response of the Adriatic Sea to the Bora and sirocco forcing, *Cont. Shelf Res.*, *14*, 91–116, doi:10.1016/0278-4343(94)90007-8.

Parish, T. P. (1982), Barrier winds along the Sierra Nevada Mountains, *J. Appl. Meteorol.*, *21*, 925–930, doi:10.1175/1520-0450(1982)021<0925:BWATSN>2.0.CO;2.

Pullen, J. Doyle, R. Hodur, A. Ogston, J. Book, H. Perkins, and R. Signell (2003), Coupled ocean-atmosphere nested modeling of the Adriatic Sea during winter and spring 2001, *J. Geophys. Res.*, *108*(C10), 3320, doi:10.1029/2003JC001780.

Pullen, J., J. Doyle, and R. P. Signell (2006), Two-way air-sea coupling: A study of the Adriatic, *Mon. Weather Rev.*, *134*(5), 1465–1483, doi:10.1175/MWR3137.1.

Pullen, J., J. Doyle, J. Haack, C. Dorman, R. P. Signell, and C. Lee (2007), Bora event variability and the role of air-sea feedback, *J. Geophys. Res.*, *112*, C03S18, doi:10.1029/2006JC003726.

Quilfen, Y., B. Chapron, T. Elfouhaily, K. Katsaros, and J. Tournadre (1998), Observation of tropical cyclones by high-resolution scatterometry, *J. Geophys. Res.*, *103*(C4), 7767–7786, doi:10.1029/97JC01911.

Signell, R. P., S. Carniel, L. Cavalieri, J. Chiggiato, J. Doyle, J. Pullen, and M. Sclavo (2005), Assessment of wind quality for oceanographic modeling in semienclosed basins, *J. Mar. Syst.*, *53*, 217–233, doi:10.1016/j.jmarsys.2004.03.006.

Smith, R. B. (1985), On severe downslope winds, *J. Atmos. Sci.*, *42*, 2597–2603, doi:10.1175/1520-0469(1985)042<2597:OSDW>2.0.CO;2.

Smith, R. B. (1987), Aerial observations of the Yugoslavian Bora, *J. Atmos. Sci.*, *44*, 269–297, doi:10.1175/1520-0469(1987)044<0269:AOOTYB>2.0.CO;2.

Steppeler, J., G. Doms, U. Schättler, H. W. Bitzer, A. Gassmann, U. Damrath, and G. Gregoric (2003), Meso-gamma scale forecasts using the nonhydrostatic model LM, *Meteorol. Atmos. Phys.*, *82*, 75–96, doi:10.1007/s00703-001-0592-9.

Stoffelen, A., and D. Anderson (1997), Scatterometer data interpretation: Estimation and validation of the transfer function CMOD4, *J. Geophys. Res.*, *102*(C3), 5767–5780, doi:10.1029/96JC02860.

Thompson, D., and R. Beal (2000), Mapping of mesoscale and submesoscale wind fields using synthetic aperture radar, Johns Hopkins APL Tech. Dig., *21*, 58–67.

Thompson, D., T. Elfouhaily, and B. Chapron (1998), Polarization ratio for microwave backscattering from the ocean surface at low to moderate incidence angles, in *Geoscience and Remote Sensing Symposium Proceedings*, pp. 1671–1673, IEEE, Los Alamitos, Calif.

Unal, C., P. Snoeij, and P. Swart (1991), The polarization-dependent relation between radar backscatter from the ocean surface and surface wind vectors at frequencies between 1 and 18 GHz, *IEEE Trans. Geosci. Remote Sens.*, *29*(4), 621–626, doi:10.1109/36.135824.

Vachon, P. W., and F. Dobson (1996), Validation of wind vector retrieval from ERS-1 SAR images over the ocean, *Global Atmos. Ocean Syst.*, *5*, 177–187.

Vachon, P. W., and F. Dobson (2000), Wind retrieval from RADARSAT SAR images: Selection of a suitable C-band HH polarization wind retrieval model, *Can. J. Remote Sens.*, *26*, 306–313.

Vilibić, I., and N. Supić (2005), Dense water generation on a shelf: The case of the Adriatic Sea, *Ocean Dyn.*, *55*, 403–415, doi:10.1007/s10236-005-0030-5.

Zecchetto, S., P. Trivero, B. Fiscella, and P. Pavese (1998), Wind stress structure in the unstable marine surface layer detected by SAR, *Boundary Layer Meteor.*, *86*, 1–28.

F. Askari, J. Chiggiato, and J. Horstmann, NATO Undersea Research Centre, Viale San Bartolomeo 400, I-19138 La Spezia, Italy.

J. D. Doyle, Naval Research Laboratory, 7 Grace Hopper Ave., Stop 2, Monterey, CA 93943, USA.

J. Pullen, Stevens Institute of Technology, 1 Castle Point on Hudson, Hoboken, NJ 07030, USA.

R. P. Signell (corresponding author), USGS Woods Hole Coastal and Marine Science Center, 384 Woods Hole Rd., Woods Hole, MA 02543, USA. (rsignell@usgs.gov)